frontiers | Frontiers in Medicine

TYPE Original Research
PUBLISHED 15 June 2023
DOI 10.3389/fmed.2023.1107128

OPEN ACCESS

EDITED BY
D. Thirumal Kumar,
Meenakshi Academy of Higher Education and Research, India

REVIEWED BY
Jin Wu,
University at Buffalo, United States
Ronald Lubet,
National Cancer Institute (NIH), United States

*CORRESPONDENCE
Sivakumar Arumugam
✉ siva_kumar.a@vit.ac.in

RECEIVED 24 November 2022
ACCEPTED 11 April 2023
PUBLISHED 15 June 2023

CITATION
Ramalingam PS, Priyadharshini A, Emerson IA and Arumugam S (2023) Potential biomarkers uncovered by bioinformatics analysis in sotorasib resistant-pancreatic ductal adenocarcinoma. *Front. Med.* 10:1107128. doi: 10.3389/fmed.2023.1107128

Potential biomarkers uncovered by bioinformatics analysis in sotorasib resistant-pancreatic ductal adenocarcinoma

Prasanna Srinivasan Ramalingam[1], Annadurai Priyadharshini[2], Isaac Arnold Emerson[2] and Sivakumar Arumugam[1]*

[1]Protein Engineering Lab, School of Biosciences and Technology, Vellore Institute of Technology, Vellore, India, [2]Bioinformatics Programming Laboratory, Department of Biotechnology, School of Biosciences and Technology, Vellore Institute of Technology, Vellore, Tamil Nadu, India

Background: Mutant KRAS-induced tumorigenesis is prevalent in lung, colon, and pancreatic ductal adenocarcinomas. For the past 3 decades, KRAS mutants seem undruggable due to their high-affinity GTP-binding pocket and smooth surface. Structure-based drug design helped in the design and development of first-in-class KRAS G12C inhibitor sotorasib (AMG 510) which was then approved by the FDA. Recent reports state that AMG 510 is becoming resistant in non-small-cell lung cancer (NSCLC), pancreatic ductal adenocarcinoma (PDAC), and lung adenocarcinoma patients, and the crucial drivers involved in this resistance mechanism are unknown.

Methods: In recent years, RNA-sequencing (RNA-seq) data analysis has become a functional tool for profiling gene expression. The present study was designed to find the crucial biomarkers involved in the sotorasib (AMG 510) resistance in KRAS G12C-mutant MIA-PaCa2 cell pancreatic ductal adenocarcinoma cells. Initially, the GSE dataset was retrieved from NCBI GEO, pre-processed, and then subjected to differentially expressed gene (DEG) analysis using the limma package. Then the identified DEGs were subjected to protein–protein interaction (PPI) using the STRING database, followed by cluster analysis and hub gene analysis, which resulted in the identification of probable markers.

Results: Furthermore, the enrichment and survival analysis revealed that the small unit ribosomal protein (RP) RPS3 is the crucial biomarker of the AMG 510 resistance in KRAS G12C-mutant MIA-PaCa2 cell pancreatic ductal adenocarcinoma cells.

Conclusion: Finally, we conclude that RPS3 is a crucial biomarker in sotorasib resistance which evades apoptosis by MDM2/4 interaction. We also suggest that the combinatorial treatment of sotorasib and RNA polymerase I machinery inhibitors could be a possible strategy to overcome resistance and should be studied in *in vitro* and *in vivo* settings in near future.

KEYWORDS

sotorasib, KRAS G12C inhibitor, resistance, pancreatic ductal adenocarcinoma, ribosomal proteins, precision medicine

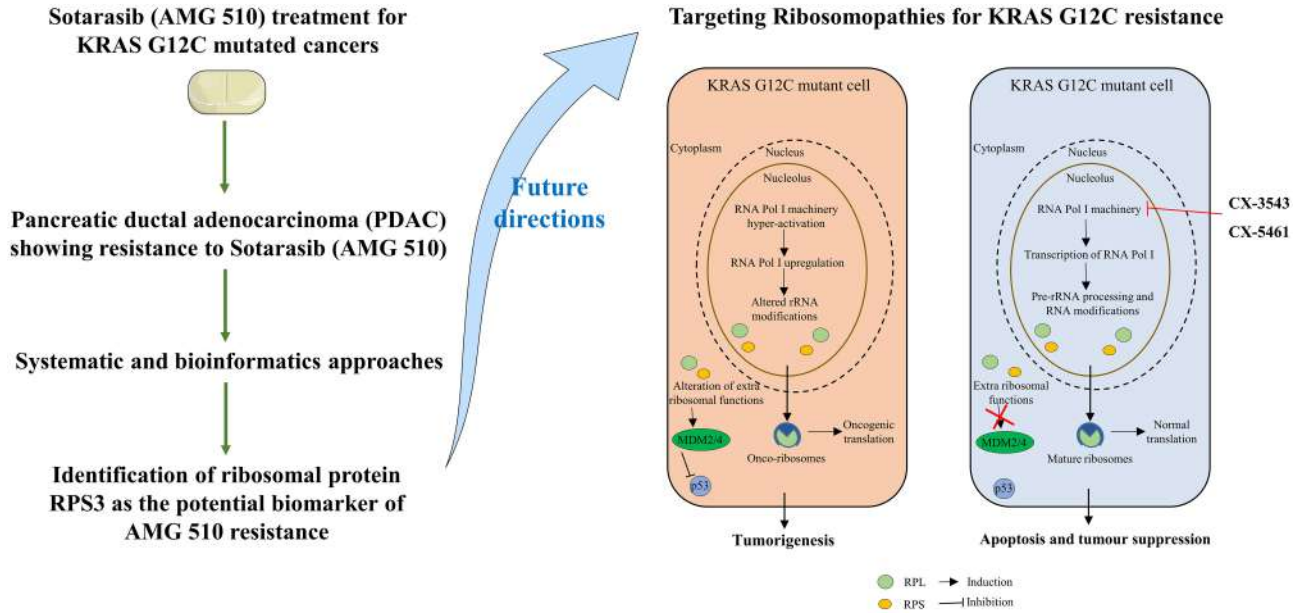

GRAPHICAL ABSTRACT
Study outcomes and proposed future directions to combat sotorasib resistance in KRAS G12C mutant cells.

1. Introduction

Mutant RAS-harboring cancers are predominant in many cancers including pancreatic, breast, colon, and lung, which corresponds to nearly 30% of all cancers (1, 2). Unlike NRAS and HRAS isoforms of RAS, the KRAS isoform has high mutation frequencies at mutational hotspots G12 (89%), G13 (9%), and Q61 (1%) residues (3–5). Overall, the G12th residue is the most mutated position of KRAS with G12D as the most prevalent mutation with 36%, followed by the G12V and G12C mutations with 23 and 14%, respectively (6). KRAS is a small GTPase that acts as a molecular switch by GTP-bound (active form) and GDP-bound (inactive form) states and triggers the downstream signal transduction pathways (7, 8). The GDP to GTP conversion is mediated by the guanine nucleotide exchange factors (GEFs), and the GTP to GDP hydrolysis is mediated by GTPase-activating proteins (GAPs) (9, 10). The mutant KRAS maintains the GTP-bound active state and overcomes the GTPase activity and initiates nearly 80 different downstream effector signaling pathways including MAPK and PI3K-mTOR signaling which further activates JUN and MYC transcription factors and promotes the cancer cell survival and proliferation (11–15).

Several strategies have been carried out to inhibit the mutant KRAS signaling such as targeting the upstream effectors (EGFR inhibitors, FGFR1 inhibitors, and IGF1R inhibitors); targeting the inhibitors of KRAS regulators (SOS1 inhibitors and SHP2 inhibitors); direct targeting of KRAS (KRAS on state and off-state inhibitors); downstream effector inhibitors (PI3K inhibitors, mTOR inhibitors, and MEK inhibitors); and cell cycle arrest (CDK4/6 inhibitors) (16–19). Moreover, targeting the other mediators and effectors in the MAPK pathway result in the signaling crosstalk such as MEK-PI3K, RAF-AKT, RAS-SKF, RAS-YAP, and SHP2-dependent MAPK reactivation and SHP2-independent PI3K reactivation (20–22). All the strategies have shown significant outcomes, but the complete inhibition of KRAS was promising in the direct targeting strategy. In general, the intracellular levels of GTP are in micromolar (μM) ranges, and its binds with picomolar (pM) affinity to the GTP-binding pocket of the KRAS, which challenges it as undruggable to the medicinal chemistry and drug discovery researchers to design and develop a potent KRAS mutant small molecule inhibitors (23–25). Finally, the undruggable became druggable by the successful discovery and FDA approval of KRAS G12C inhibitor sotorasib (AMG 510) for the treatment of non-small-cell lung cancer (NSCLC) and other solid tumors (26–28). The sotorasib specifically targets the cryptic pocket of the KRAS G12C (H95/Y96/Q99) and forms the covalent bond with the reactive cysteine at the 12th position, which also limits its ability to target other KRAS mutants such as G12D and G12V that lacks reactive cysteine (29). Recently, in December 2022, FDA granted the accelerated approval for adagrasib (MRTX849) for the treatment of KRAS G12C-mutated NSCLC (30).

Accumulating pieces of evidence report that sotorasib is becoming resistant among NSCLC, pancreatic ductal adenocarcinoma, and colorectal adenocarcinoma patients bearing KRAS G12C mutation and even resulting in hepatotoxicity (31, 32). The understanding of this resistance mechanism is challenging due to the intracellular heterogeneity and variability of KRAS G12C-mutated cancer cells (33). Hence, to identify the crucial biomarkers involved in the sotorasib resistance, we have retrieved the RNA-seq data from the NCBI GEO database of AMG 510 treated (resistant) and untreated in KRAS G12C-mutant MIA-PaCa2 pancreatic ductal adenocarcinoma cells. The differentially expressed genes (DEGs) were identified by the linear model, and then, the DEGs were subjected to protein–

protein interaction (PPI), cluster analysis, and hub gene analysis. In addition to this, the resulting probable biomarkers were also subjected to gene ontology (GO), pathway enrichment, and survival analyses to find the crucial biomarker in the sotorasib resistance.

2. Materials and methods

2.1. Data collection and pre-processing

The RNA-seq dataset retrieved for this study was accessed through NCBI Gene Expression Omnibus (GEO) database (http://www.ncbi.nlm.nih.gov/geo/). The keywords used for filtering the dataset include "KRAS mutated Pancreatic cancer" and "*Homo sapiens*" (organism). The datasets were screened, and "GSE178479" was retrieved for this study in which the sotorasib (AMG 510) resistance in the KRAS G12C-mutant MIA-PaCa2 pancreatic ductal adenocarcinoma cells was reported (34). The sequencing platform and the platform ID of the sample were "Illumina HiSeq 4000" and "GPL20301," respectively. The number of samples used in this study was two, which includes RNA-seq profiles of AMG 510 treated (rep1 and rep2) and AMG 510 untreated (rep1 and rep2) MIA-PaCa2 cells. The present study was carried out to predict the crucial biomarkers involved in the AMG 510 resistance in pancreatic ductal adenocarcinoma cells.

The count matrix of the samples was prepared based on the matrix file information provided in the GEO database (35). The lowly expressed genes were filtered based on their counts using the counts per million (CPM) function in the *edgeR* package with the threshold of 0.5. Box plots were used to check the distribution of the read counts on the log2 scale (36). The CPM function provided the log2 counts per million which are then corrected for different library sizes. The CPM function also adds a small offset to avoid taking a log of zero. The trimmed mean of M-value (TMM) normalization was performed to eliminate composition biases between the libraries (37). This generates a set of normalization factors, where the product of these factors and the library sizes define the effective library size. The *calcNormFactors* function calculated the normalization factors between libraries.

2.2. Differential gene expression analysis

The *limma* package (38, 39) with the voom function was used, which transforms the read counts into logCPMs while taking account of the mean–variance relationship in the given data (40, 41). After vooming, we applied a linear model to the voom transformed data to test for differentially expressed genes (DEGs) using standard *limma* commands.

The voom transformed data have been used in *limma* to test for differential gene expression. The linear model fit was designed for each gene using the lmFit function in *limma* which estimates the groups and gene-wise variances. The contrast between the groups was then analyzed based on the makeContrasts function. Then the contrasts matrix was fitted to the object to get the statistics and estimated parameters. Here, we called the contrasts.fit function in *limma*. Furthermore, we called the eBayes function to perform the empirical Bayes shrinkage on the variances and estimated the logFC of 0.05 and their associated *p*-values. Finally, to increase the significance and reduce the false discovery rates, we used the TREAT function to predict specific genes (42–44).

2.3. Network analysis

The differentially expressed genes (DEGs) filtered through the TREAT function were then subjected to the STRING database (https://string-db.org/) to predict the protein–protein interactions (PPIs) with a confidence level of 0.004 and higher, and the first shell of 10 interactions was used as a filter (45). The MCODE and CytoHubba were used to analyze the probable marker genes among the DEGs (46).

2.4. Enrichment and survival analysis

The hub genes resulting from the network analysis were then subjected to gene ontology using the enrichGO function in the clusterProfiler package (47). The enriched biological process (BP), cellular components (CC), and molecular functions (MF) were analyzed using the enrichGO function. The KEGG pathway analysis was also carried out using the enrichKEGG function to analyze the enriched terms.

The Kaplan–Meier (KM) survival analysis was carried out based on the Spearman correlation using the Kaplan–Meier plotter online tool employing the median patient splitting mode (48, 49). Hazard is the defined slope for the survival curve which measures the incidence of death, and the hazard ratio (HR) compares the two treatment groups. If HR is 2.0, then the rate of death in one treatment group is twice the other group (50). A statistical hypothesis test was calculated based on a log-rank test. The schematic representation of the workflow of the study is shown in Figure 1.

3. Results

3.1. Identification of differently expressed genes

Through *limma* analysis, we have tested the difference between the sotorasib (AMG 510) treated and untreated samples to analyze the genes responsible for the AMG 510 resistance in the treated group. The voom transformation of adjusting the library size with the normalization factors was analyzed through a mean–variance trend. The comparative boxplot analysis of unnormalized logCPM with the voom transformed logCPM is shown in Figure 2 which represents the precision of normalization. The CPM plot of count data after filtering the lowly expressed genes is provided in Supplementary Figure 1. The mean–variance relationship helps to analyze whether the low counts are filtered adequately and variation in the data by estimating the relationship of the log counts, which generates a precision weight for each observation and enters these into the limma empirical Bayes analysis. The voom mean–variance trend curve is shown in Supplementary Figure 2.

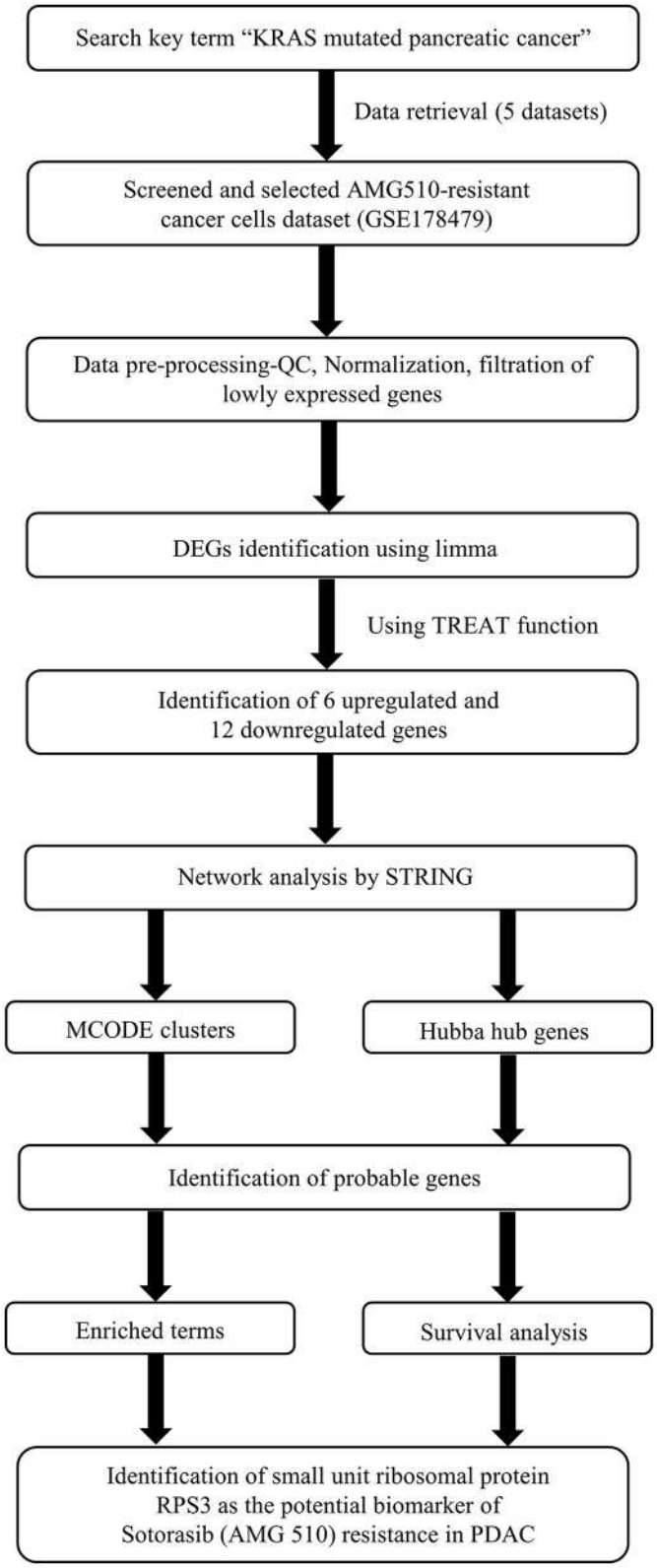

FIGURE 1
Schematic representation of the workflow of the study.

The empirical Bayes function was used to analyze the DEGs with the linear model fit. The linear model fit resulted in the identification of upregulated and downregulated genes from the DEGs. In this study, it resulted in the differentially expressed genes among the AMG 510 treated (resistant) and untreated groups, which are repressed through the MA plot as shown in Figure 3 and

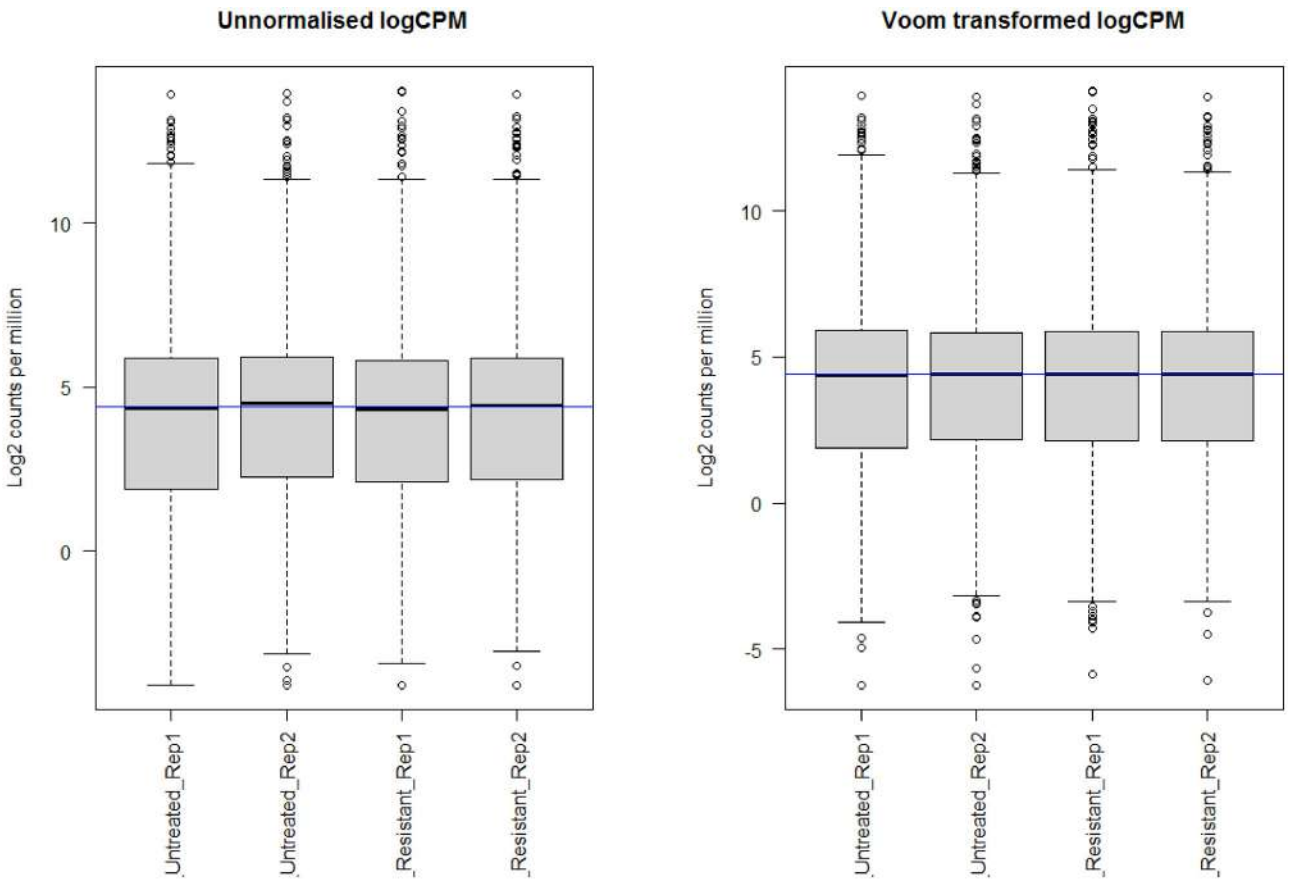

FIGURE 2
Boxplot analysis of unnormalized logCPM with the voom transformed logCPM.

the volcano plot as shown in Figure 4. Initially, the raw RNA-seq data were retrieved, pre-processed, and the differentially expressed genes (DEGs) were predicted using a cutoff on the log fold change threshold of 0.5. The *p*-value threshold of 0.05 resulted in the identification of 330 upregulated genes and 499 downregulatory genes as shown in Figure 4, and the complete list of DEGs is provided in Supplementary Table 1. To reduce false discovery rates, we further applied TREAT (*t*-tests relative to a threshold) function in the limma package, which resulted in the identification of six upregulated DEGs and 12 downregulated DEGs.

3.2. Network analysis

The interaction network was visualized using Cytoscape using molecular complex detection (MCODE) to find the significant clusters between each node representing a gene while edges represent the interaction of the molecules. The default parameters were set including the degree cutoff of 2, node score cutoff of $\geq$0.2, K-score of $\geq$2, and max depth from seed of 100. Finally, the MCODE resulted in six clusters with the highest nodal score of 22 as shown in Figure 5.

The probable marker genes have been identified based on the highly connected nodes using CytoHubba in Cytoscape. It uses 12 scoring methods to identify the markers, namely, betweenness, bottleneck, closeness, clustering coefficient (CC), degree, the density of maximum neighborhood component (DMNC), eccentricity (EcC), edge percolated component (EPC), maximal clique centrality (MCC), maximum neighborhood component (MNC), radiality, and stress. The top 10 genes from each scoring method were isolated. Genes that are common in more than five scoring methods and also have an impact on MCODE were considered hub genes.

3.3. Enrichment analysis

The enrichment analysis was performed with the GO terms: biological process (BP), cellular components (CC), and molecular functions (MF). The biological process includes cytoplasmic translation, ribosomal small subunit assembly, ribosome assembly, ribosomal small subunit biogenesis, non-membrane-bounded organelle assembly, negative regulation of protein ubiquitination, and negative regulation of protein modification by small protein conjugation or removal. Cellular components include cytosolic ribosome, ribosomal subunit, ribosome, cytosolic small ribosomal subunit, cytosolic large ribosomal subunit, small ribosomal subunit, large ribosomal

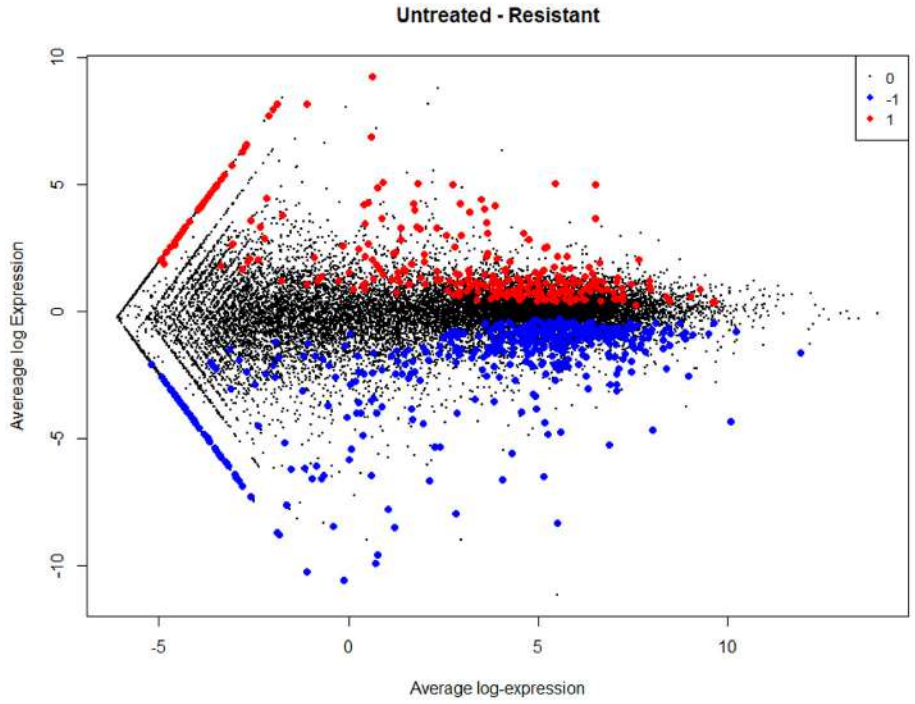

FIGURE 3
MA plot used to represent log fold change vs. mean expression between the two groups (AMG 510 treated and untreated). A scatter plot depicts the normalized mean expression on the x-axis and base-2 log fold change on the y-axis. The red dots represent the upregulated genes, the blue dots represent the downregulated genes, and the black dots represent the non-significant genes.

subunit, focal adhesion, cell–substrate junction, polysome, polysomal ribosome, rough endoplasmic reticulum, cytoplasmic side of endoplasmic reticulum membrane, rough endoplasmic reticulum membrane, and euchromatin. Molecular functions are structural constituents of the ribosome and rRNA binding. The enriched GO terms of biological process (BP), cellular components (CC), and molecular functions (MF) are shown in Figure 6 and Table 1. Then the KEGG pathway analysis was also carried out, and the enriched term was observed as "hsa03010:Ribosome."

3.4. Survival analysis

The Kaplan–Meier (KM) survival analysis plot was created based on Spearman's correlation, using the hazard ratio (HR) and log-rank test of the genes. In general, HR $>$ 1 represents that the low-expression group has a higher chance of survival than the high-expression group, and HR $<$ 1 represents that high-expression groups have a higher chance of survival than the low-expression group. The survival analysis of probable genes showed that the low expression of RPL4, RPL32, RPLP1, and RPS3 would have a higher probability for survival, and the high expression of RPS28, RPS15, RPS9, RPL15, and JUN would have a higher probability for survival. Based on the log-rank test, the significance level was set to 0.05, and if the calculated p-value is $>$0.05, the null hypothesis is retained. Based on these criteria, the ribosomal protein RPS3 was identified as a probable biomarker that showed high survival rates and $p < 0.05$ as shown in Figure 7. In addition, the HR of RPS3 is almost near two which indicates that it has twice the rate of death when compared to the others. The KM survival plots of RPL15, RPS15, RPS28, RPL4, RPL32, RPLP1, RPS9, and JUN are shown in Supplementary Figure 3.

4. Discussion

KRAS mutations are prevalent in many cancers including pancreatic, breast, colon, and lung with mutational hotspots at G12 (89%), G13 (9%), and Q61 (1%) residues (1, 2). The G12D, G12C, and G12V are frequent mutations with 36, 23, and 14% expressions, respectively (6). Of note, the KRAS G12C mutation is relatively high in lung adenocarcinoma than in pancreatic adenocarcinoma patients. The direct inhibition of the mutant KRAS is very prominent over other strategies but challenges the small molecule inhibitor development due to their high-affinity GTP-binding pocket and smooth surface (16, 51). Structure-based drug design guided the development and FDA approval of first-in-class potential KRAS G12C inhibitor sotorasib (AMG 510) that has changed the scenario in which the mutant KRAS became undruggable (26). Recently, in December 2022, FDA granted the accelerated approval for Adagrasib (MRTX849) for the treatment of KRAS G12C-mutated NSCLC (30). In addition to this, several pharma industries have initiated to design and develop novel KRAS mutant inhibitors (mutant specific/pan-KRAS). Several KRAS G12C (GDP-bound off state) inhibitors, such as sotorasib

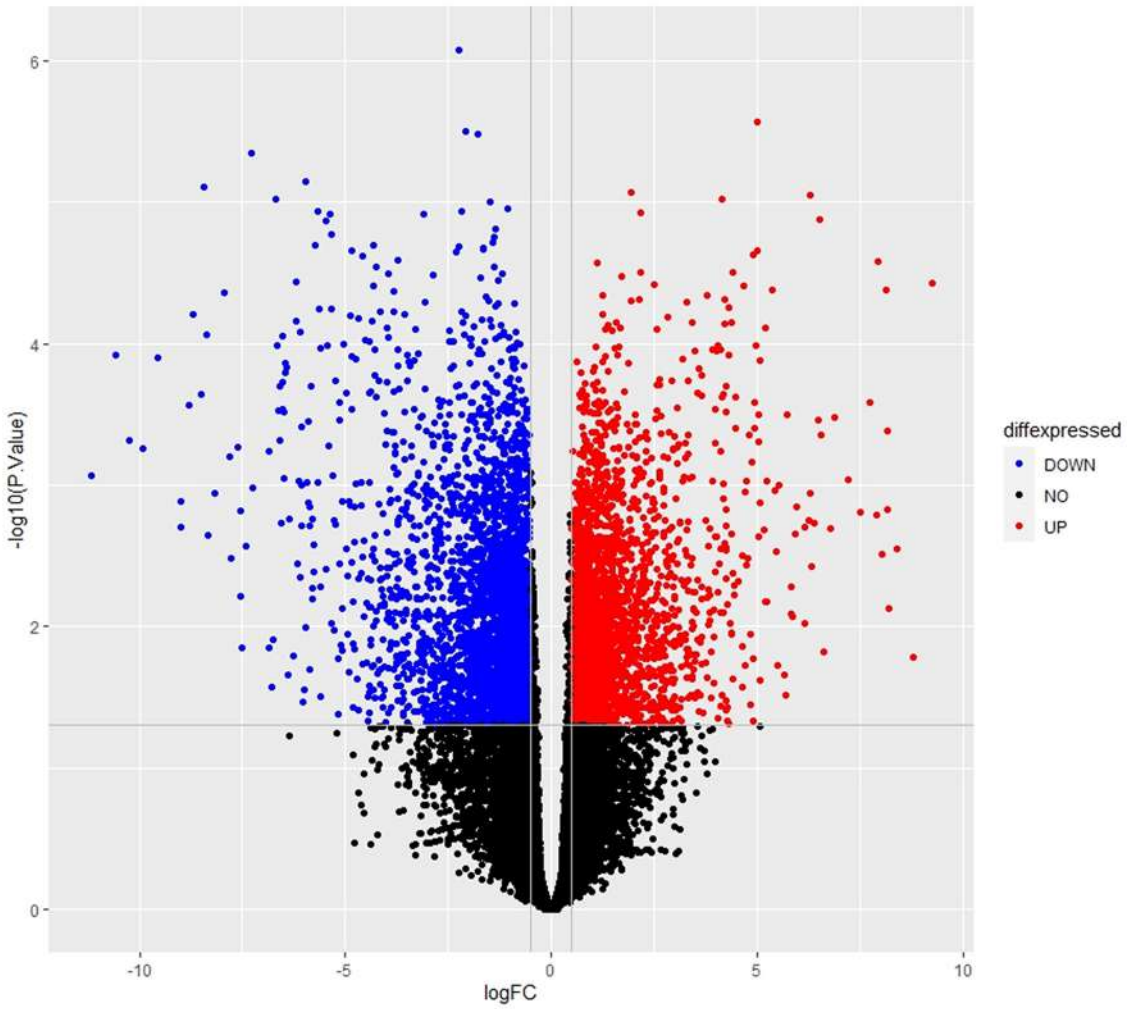

FIGURE 4
Volcano plot of the DEGs depicts the logFC on the *x*-axis and −log10 (*p*-value) on the *y*-axis. The red dots represent the upregulated genes, the blue dots represent the downregulated genes, and the black dots represent the non-significant genes.

(AMG 510), adagrasib (MRTX849), GDC-6036, JNJ-74699157, D-1553, JDQ443, LY3537982, LY3499446, ARS1620, and KRAS G12C (GDP-bound off state) inhibitors such as RMC-6291, RMC-6236, and RM-018, and Pan KRAS Switch I/II inhibitors such as BI-2852, are being studied in preclinical and clinical studies (18, 52–55). Recent pieces of evidence report the resistance to AMG 510 among KRAS G12C-mutant cancer patients (31, 33). Moreover, Adagrasib (MRTX849) and ARS1620 were reported to have acquired resistance in KRAS G12C-mutant cells (33, 56). Amplification of the mesenchymal epithelial transition factor receptor (MET); activating mutations of downstream effectors, such as BRAF, and dual specificity mitogen-activated protein kinase kinase 1 (MEK1); oncogenic fusion with fibroblast growth factor receptor 3 (FGFR3) and CCDC6-RET; and loss-of-function mutations of phosphatase and tensin homolog (PTEN) and neurofibromin 1 (NF1) were reported to be the key elements involved in the resistance mechanisms to KRAS mutant inhibitors in lung adenocarcinoma and colorectal adenocarcinoma (56, 57). Unlike the abovementioned resistance mechanisms, our results revealed a significant correlation between the sotorasib resistance in KRAS G12C-mutant cells and ribosomopathies.

Recently Chan et al. (34) reported an interesting study on the identification of sotorasib (AMG 510) resistance in the KRAS G12C-mutant MIA-PaCa2 pancreatic ductal adenocarcinoma cells when treated with increasing dosage (0.1–5 μM) for 60 days and found that MIA-PaCa2 showed resistance at 5 μM treatment of AMG 510 (34). This interested us to identify the crucial biomarkers involved in the AMG 510 resistance in the KRAS G12C-mutant MIA-PaCa2 pancreatic ductal adenocarcinoma cells. In addition to MIA-PaCa2 cells, they have also tested the AMG 510 resistance in SW1463 human Caucasian rectum adenocarcinoma, LU99 lung giant cell carcinoma, and LU65 lung carcinoma cell lines which have KRAS G12C mutations.

The main aim of the present study was to identify the key biomarker genes involved in the AMG 510 resistance. Initially, the raw RNA-seq data were retrieved, pre-processed, and the differentially expressed genes (DEGs) were predicted

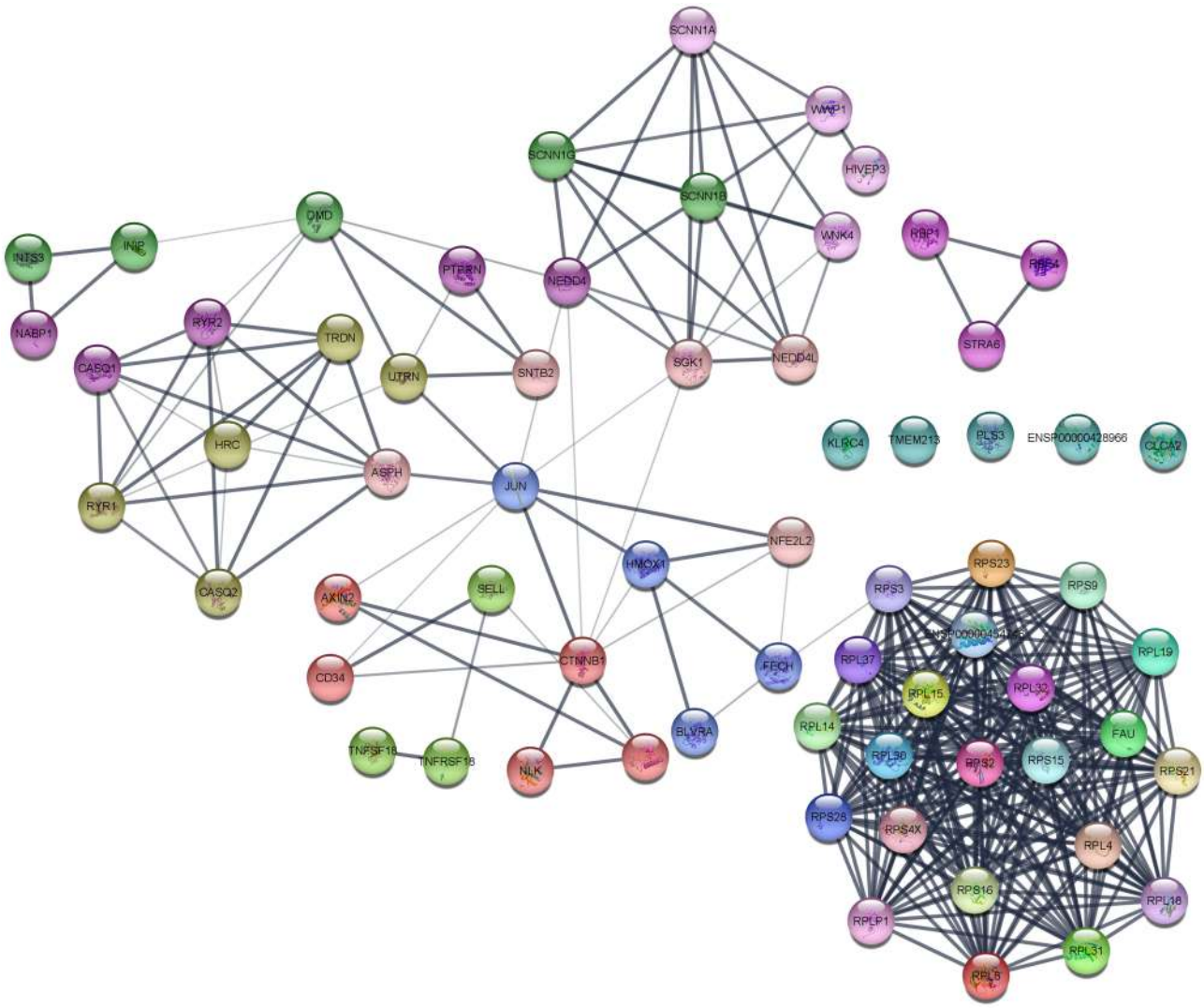

FIGURE 5
Protein–protein interaction (PPI) network of DEGs obtained from the STRING database.

which resulted in the identification of 330 upregulated genes and 499 downregulatory genes as shown in Figure 4 and Supplementary Table 1. The *t*-tests relative to a threshold (TREAT) function reduced the false discovery rates of DEGs (42), which further resulted in the identification of six upregulated and 12 downregulated genes. These filtered DEGs were studied for the protein–protein interaction network using STRING which resulted in four MCODE clusters, and the MCODE cluster 1 showed the highest nodal density among the other clusters as shown in Figure 5. In addition, cluster analysis and hub gene analysis were carried out which resulted in probable biomarkers as shown in Figure 6, and the enriched GO terms of biological process (BP), cellular components (CC), and molecular functions (MF) are shown in Table 1. In general, HR $>$ 1 represents that the low-expression group has a high chance of survival than the high-expression group, and HR $<$ 1 represents that the high-expression group has a high chance of survival than the low-expression group (58). Finally, the survival analysis based on the hazard ratio and log-rank test resulted in the identification of RPS3 as the probable biomarker with high survival rates and $p < 0.05$ as shown in Figure 7. Based on the log-rank test, the significance level was set to 0.05, and if the calculated p-value is >0.05, the null hypothesis is retained. Moreover, the HR of RPS3 is nearly 2 which indicates that it has twice the rate of death when compared to the others. The KM survival plots of RPL15, RPS15, RPS28, RPL4, RPL32, RPLP1, RPS9, and JUN are shown in Supplementary Figure 3. In addition, the GO of all the 330 upregulated genes and 499 downregulatory genes shown in Supplementary Table 1 reveals that the myc transcriptional targets, such as E2F transcription factor 6 (ENSG00000169016), are upregulated and the CDK10 (ENSG00000185324) is downregulated. Generally, the E2F6 regulates the gene expression of proteins involved in cell proliferation and the CDK10 acts as a tumor suppressor.

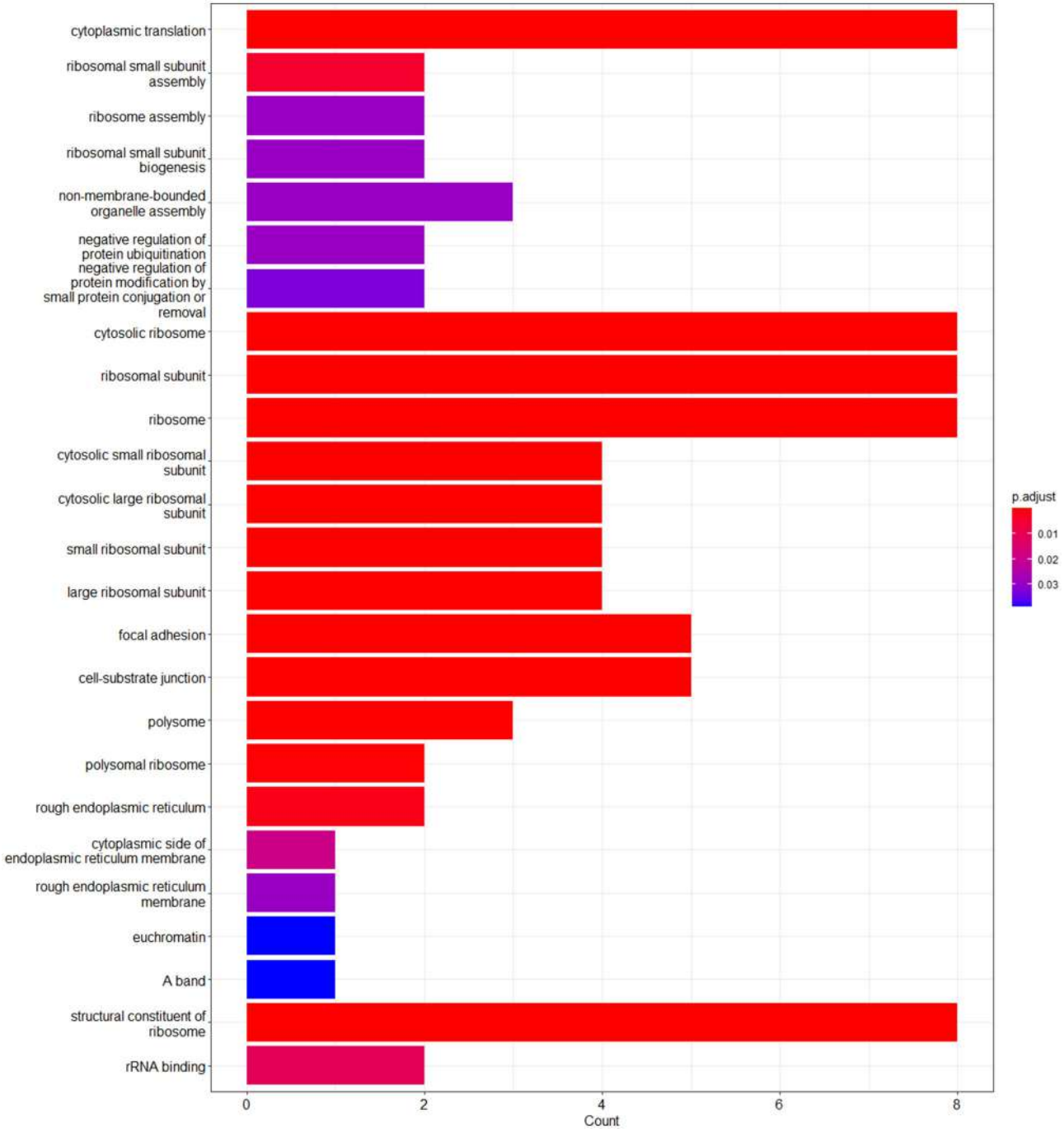

FIGURE 6
Bar plot of the enriched GO terms analyzed using enrichGO function using cluster profiler.

Furthermore, the CDC25B (ENSG00000101224) expression has a p53-dependent tumor suppressive effect, which is downregulated. The anti-apoptotic BCL-6 (ENSG00000113916) is downregulated. The abovementioned targets are also involved in the RAS signaling pathway. These data suggest that the resistance could be a result of RNA pol I machinery hyperactivation and apoptosis evasion. The present study revealed that the small unit ribosomal protein RPS3 is known to be only expressed in the AMG 510 resistant MIA-PaCa2 cells and identified as a significant biomarker involved in the resistance of AMG 510. These novel identifications resulted from the emergence and accumulation of RNA-Seq data of drug-resistant cancer cells.

Ribosome biogenesis starts from the nucleolus and ends in the cytoplasm with the formation of the mature ribosome from rRNA and ribosomal proteins (59). In normal cells, the RNA pol I initiates the Pol I transcription followed by the pre-rRNA processing and modification and then assembled

10.3389/fmed.2023.1107128

TABLE 1 Gene ontology analysis of the enriched terms.

GO term and GO ID	DEGs	*p*-value	Adjusted *p*-value	Genes
Cytoplasmic translation (GO:0002181)	BP	1.13E-16	2.91E-14	RPL4/RPLP1/RPS28/RPS9/RPL32/RPL15/RPS15/RPS3
Ribosomal small subunit assembly (GO:0000028)	BP	3.50E-05	0.004512	RPS28/RPS15
Ribosome assembly (GO:0042255)	BP	0.00037	0.029458	RPS28/RPS15
Ribosomal small subunit biogenesis (GO:0042274)	BP	0.00053	0.029458	RPS28/RPS15
Non-membrane-bounded organelle assembly (GO:0140694)	BP	0.000575	0.029458	RPS28/RPS15/RPS3
Negative regulation of protein ubiquitination (GO:0031397)	BP	0.000685	0.029458	RPS15/RPS3
Negative regulation of protein modification by small protein conjugation or removal (GO:1903321)	BP	0.000896	0.033031	RPS15/RPS3
Cytosolic ribosome (GO:0022626)	CC	3.72E-18	1.34E-16	RPL4/RPLP1/RPS28/RPS9/RPL32/RPL15/RPS15/RPS3
Ribosomal subunit (GO:0044391)	CC	3.95E-16	7.10E-15	RPL4/RPLP1/RPS28/RPS9/RPL32/RPL15/RPS15/RPS3
Ribosome (GO:0005840)	CC	4.09E-15	4.91E-14	RPL4/RPLP1/RPS28/RPS9/RPL32/RPL15/RPS15/RPS3
Cytosolic small ribosomal subunit (GO:0022627)	CC	2.30E-09	2.07E-08	RPS28/RPS9/RPS15/RPS3
Cytosolic large ribosomal subunit (GO:0022625)	CC	8.69E-09	6.26E-08	RPL4/RPLP1/RPL32/RPL15
Small ribosomal subunit (GO:0015935)	CC	1.98E-08	1.19E-07	RPS28/RPS9/RPS15/RPS3
Large ribosomal subunit (GO:0015934)	CC	1.30E-07	6.71E-07	RPL4/RPLP1/RPL32/RPL15
Focal adhesion (GO:0005925)	CC	5.12E-07	2.23E-06	RPL4/RPLP1/RPS9/RPS15/RPS3
Cell-substrate junction (GO:0030055)	CC	5.56E-07	2.23E-06	RPL4/RPLP1/RPS9/RPS15/RPS3
Polysome (GO:0005844)	CC	3.04E-06	1.10E-05	RPS28/RPL32/RPS3
Polysomal ribosome (GO:0042788)	CC	9.28E-05	0.000304	RPS28/RPL32
Rough endoplasmic reticulum (GO:0005791)	CC	0.000614	0.001842	RPL4/RPS28
Cytoplasmic side of endoplasmic reticulum membrane (GO:0098554)	CC	0.006886	0.019069	RPS28
Rough endoplasmic reticulum membrane (GO:0030867)	CC	0.011453	0.029451	RPS28
Euchromatin (GO:0000791)	CC	0.017363	0.039066	JUN
A band (GO:0031672)	CC	0.017363	0.039066	RPL15
Structural constituent of ribosome (GO:0003735)	MF	7.11E-16	3.34E-14	RPL4/RPLP1/RPS28/RPS9/RPL32/RPL15/RPS15/RPS3
rRNA binding (GO:0019843)	MF	0.000478	0.011236	RPS9/RPS3

with ribosomal proteins (RPs) to form mature 60s and 40s subunits and ultimately takes part in protein synthesis. Unlike normal cells, the RNA pol I is hyperactivated leading to the altered rRNA modifications and altered RPs extraribosomal functions, thus forming the onco-ribosomes and translating the oncogenic mRNAs and ultimately ending with ribosomopathies (59). Some large subunit ribosomal proteins, such as RPL5, RPL9, RPL10, RPL11, RPL15, RPL21, RPL22, RPL23A, RPL27, RPL31 RPL34, RPL35, RPL36, and large subunit ribosomal proteins, such as RPS7, RPS15, RPS15A, RPS17, RPS19, RPS20, RPS24, RPS27, and RPSA, are reported to have significant roles in the progression of various types of cancers including lung, colon, breast, and pancreatic cancers (60–62). Generally, the ribosomal proteins (RPs) directly/indirectly interact with the Mdm2/Mdm4 E3 ubiquitin-protein ligases, which in turn regulate the degradation of p53 tumor suppressor protein resulting in the tumor progression (62, 63). An interesting study reports that the WD repeat-containing protein 74 (WDR74) alters the RPL5 levels and promotes metastasis by degrading p53 via the RPS15-Mdm2 axis in

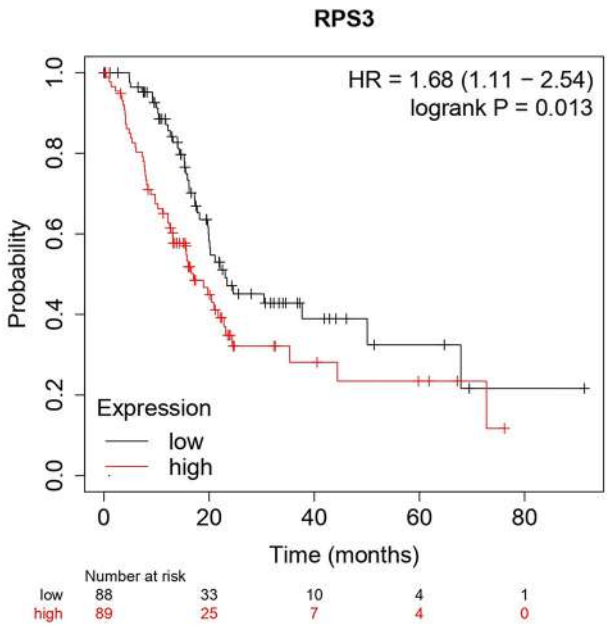

FIGURE 7
The Kaplan–Meier plot for survival analysis of key biomarkers RPS3. The *x*-axis represents the time in months, while the *y*-axis represents the probability of survival. The red and black colors represent the high expression and low expression of the biomarkers, respectively.

lung carcinoma (64). The ribosomal proteins were upregulated in KRAS mutant Panc-1 cells, and their inhibition results in cell cycle arrest, apoptosis induction, and antiproliferation (65, 66).

RPS3 knockdown in Caco-2 colon cancer cells showed decreased cancer progression and increased apoptosis via p53 upregulation and reduced activity of lactate dehydrogenase (LDH) (67). RPS3 was also reported to induce apoptosis by disrupting its interaction with E2F1 and also upregulates the expression of pro-survival genes in NSCLC (68). On this note, the mutations in the ribosomal proteins are also highly involved in tumorigenesis. The RPs were reported to interact with MDM2/4 and inhibit p53, and overexpression was observed as a result of the hyperactivation of RNA polymerase I machinery. The inhibition of RNA polymerase I machinery by inhibitors, such as CX-3543 and CX-5461, promotes p-53-dependent apoptosis in several cancers (69, 70). The clinical trials of RNA polymerase I machinery by inhibitors CX-5461 (NCT02719977) and CX-3543 (NCT00955786) resulted in the identification of safety, tolerable dosage, and effective dosage regimes and also resulted in less toxicity in patients (71). The potential of individual RNA polymerase I machinery inhibitors was studied, and combination strategies have to be studied in near future from the successful interventions from preclinical studies. Chan et al. (34) reported that the sotorasib resistance was offered by the PAK/PI3K pathway in KRAS G12C-mutant MIA-PaCa2 cells, and our bioinformatics analysis showed that RPS3 was the crucial biomarker. Recent reports show that RPS3 mediates the PI3K-Akt signaling axis in cancer cells, which correlates with our findings from the study (72, 73).

From the above understandings, we observe and conclude that the small unit ribosomal protein RPS3 is the crucial biomarker of the AMG 510 resistance in KRAS G12C-mutant MIA-PaCa2 cell pancreatic ductal adenocarcinoma cells. The study outcomes and the possible future directions to combat the Sotorasib resistance in KRAS G12C mutant cells were shown in the Graphical Abstract. Co-targeting of ribosomal proteins along with the target-specific inhibitors (here KRAS G12C-mutant inhibitor) will pave way for the development of precision treatment, such as using CRISPR-Cas and T-cell immunotherapy, in cancer.

5. Conclusion

The current study was performed to evaluate the crucial biomarkers involved in the KRAS G12C inhibitor, sotorasib (AMG 510). From the analysis, we finally conclude that the ribosomal protein RPS3 is the crucial biomarker involved in the AMG 510 resistance in the KRAS G12C-mutant MIA-PaCa2 cell pancreatic ductal adenocarcinoma cells. From the study results and previous literature, we also report that resistance could result from the degradation of p53 via the RPs-MDM2/MDM4-p53 axis. Thus, the combinatorial treatment strategy of (i) KRAS G12C-mutant inhibitors and (ii) RNA polymerase I machinery inhibitors, such as CX-3543 and CX-5461, could be a possible strategy to tackle resistance and has to be studied in *in vitro* and *in vivo* settings, which promotes the increased therapeutic treatment of KRAS G12C-mutated cancers in the era of precision medicine.

Data availability statement

Publicly available datasets were analyzed in this study. This data can be found here: GSE178479.

Author contributions

PSR conceptualized and designed the study. PSR and AP retrieved the data, carried out all the analyses, and wrote the manuscript. All the results were validated and the manuscript was corrected by IE and SA. All authors proofread the manuscript. All authors contributed to the article and approved the submitted version.

Funding

The authors thank Vellore Institute of Technology, Vellore for providing 'VIT SEED Grant-RGEMS Fund (SG20220095)' for carrying out this research work.

Acknowledgments

The authors would like to thank Vellore Institute of Technology (VIT), Vellore, India, for providing the necessary facilities to carry out this study.

Conflict of interest

The authors declare that the research was conducted in the absence of any commercial or financial relationships that could be construed as a potential conflict of interest.

Publisher's note

All claims expressed in this article are solely those of the authors and do not necessarily represent those of their affiliated organizations, or those of the publisher, the editors and the reviewers. Any product that may be evaluated in this article, or claim that may be made by its manufacturer, is not guaranteed or endorsed by the publisher.

Supplementary material

The Supplementary Material for this article can be found online at: https://www.frontiersin.org/articles/10.3389/fmed.2023.1107128/full#supplementary-material

SUPPLEMENTARY FIGURE 1
CPM plot of count data after filtering the poorly expressed genes.

SUPPLEMENTARY FIGURE 2
Voom mean–variance trend curve. It depicts that the lowly expressed genes are filtered properly. t. Counts nearly 0 (plot *x*-axis value −1) have low standard deviations. This rises immediately for low counts and then gradually decreases.

SUPPLEMENTARY FIGURE 3
Kaplan–Meier plot for survival analysis of RPL4 **(A)**, RPL32 **(B)**, RPLP1 **(C)**, RPS9 **(D)**, JUN **(E)**, RPL15 **(F)**, RPS15 **(G)**, and RPS28 **(H)**. The *x*-axis represents the time in months, while the *y*-axis represents the probability of survival. The red and black colors represent the high expression and low expression of the biomarkers, respectively.

References

1. Prior IA, Lewis PD, Mattos C. A comprehensive survey of Ras mutations in cancer. *Cancer Res.* (2012) 72:2457–67. doi: 10.1158/0008-5472.CAN-11-2612

2. Fernández-Medarde A, Santos E. Ras in cancer and developmental diseases. *Genes Cancer.* (2011) 2:344–58. doi: 10.1177/1947601911411084

3. Malumbres M, Barbacid M, RAS. oncogenes: the first 30 years. *Nat Rev Cancer.* (2003) 3:459–65. doi: 10.1038/nrc1097

4. Harvey JJ. An unidentified virus which causes the rapid production of tumours in mice. *Nature.* (1964) 204:1104–5. doi: 10.1038/2041104b0

5. Kirsten WH, Schauf V, McCoy J. Properties of a murine sarcoma virus. *Bibl Haematol.* (1970) 36:246–9. doi: 10.1159/000391714

6. Hobbs GA, Der CJ, Rossman KL. RASisoforms and mutations in cancer at a glance. *J Cell Sci.* (2016) 129:1287–92. doi: 10.1242/jcs.182873

7. Yin G, Kistler S, George SD, Kuhlmann N, Garvey L, Huynh M, et al. GTPase K104Q mutant retains downstream signaling by offsetting defects in regulation. *J Biol Chem.* (2017) 292:4446–56. doi: 10.1074/jbc.M116.762435

8. Colicelli J. Human RAS superfamily proteins and related GTPases. *Sci STKE.* (2004) 2004:RE13. doi: 10.1126/stke.2502004re13

9. Yorimitsu T, Sato K, Takeuchi M. Molecular mechanisms of Sar/Arf GTPases in vesicular trafficking in yeast and plants. *Front Plant Sci.* (2014) 5:411. doi: 10.3389/fpls.2014.00411

10. Cherfils J, Zeghouf M. Regulation of small GTPases by GEFs, GAPs, and GDIs. *Physiol Rev.* (2013) 93:269–309. doi: 10.1152/physrev.00003.2012

11. Takács T, Kudlik G, Kurilla A, Szeder B, Buday L, Vas V. The effects of mutant Ras proteins on the cell signalome. *Cancer Metastasis Rev.* (2020) 39:1051–65. doi: 10.1007/s10555-020-09912-8

12. Han CW, Jeong MS, Jang SB. Understand KRAS and the quest for anti-cancer drugs. *Cells.* (2021) 10:cells10040842. doi: 10.3390/cells10040842

13. Healy FM, Prior IA, MacEwan DJ. The importance of Ras in drug resistance in cancer. *Br J Pharmacol.* (2022) 179:2844–67. doi: 10.1111/bph.15420

14. Merz V, Gaule M, Zecchetto C, Cavaliere A, Casalino S, Pesoni C, et al. Targeting KRAS: the elephant in the room of epithelial cancers. *Front Oncol.* (2021) 11:638360. doi: 10.3389/fonc.2021.638360

15. Ferreira A, Pereira F, Reis C, Oliveira MJ, Sousa MJ, Preto A. Crucial role of oncogenic KRAS mutations in apoptosis and autophagy regulation: therapeutic implications. *Cells.* (2022) 11:cells11142183. doi: 10.3390/cells11142183

16. Désage A-L, Léonce C, Swalduz A, Ortiz-Cuaran S. Targeting KRAS mutant in non-small cell lung cancer: novel insights into therapeutic strategies. *Front Oncol.* (2022) 12:796832. doi: 10.3389/fonc.2022.796832

17. Huang L, Guo Z, Wang F, Fu L. KRAS mutation: from undruggable to druggable in cancer. *Signal Transduct Target Ther.* (2021) 6:386. doi: 10.1038/s41392-021-00780-4

18. Lindsay CR, Garassino MC, Nadal E, Öhrling K, Scheffler M, Mazières J. On target: rational approaches to KRAS inhibition for treatment of non-small cell lung carcinoma. *Lung Cancer.* (2021) 160:152–65. doi: 10.1016/j.lungcan.2021.07.005

19. Zhu C, Guan X, Zhang X, Luan X, Song Z, Cheng X, et al. Targeting KRAS mutant cancers: from druggable therapy to drug resistance. *Mol Cancer.* (2022) 21:159. doi: 10.1186/s12943-022-01629-2

20. Rozengurt E, Eibl G. Crosstalk between KRAS, SRC and YAP signaling in pancreatic cancer: interactions leading to aggressive disease and drug resistance. *Cancers.* (2021) 13:5126. doi: 10.3390/cancers13205126

21. Adachi Y, Kimura R, Hirade K, Ebi H. Escaping KRAS: gaining autonomy and resistance to KRAS inhibition in KRAS mutant cancers. *Cancers.* (2021) 13:cancers13205081. doi: 10.3390/cancers13205081

22. Sun C, Hobor S, Bertotti A, Zecchin D, Huang S, Galimi F, et al. Intrinsic resistance to MEK inhibition in KRAS mutant lung and colon cancer through transcriptional induction of ERBB3. *Cell Rep.* (2014) 7:86–93. doi: 10.1016/j.celrep.2014.02.045

23. Nagasaka M, Li Y, Sukari A, Ou S-HI, Al-Hallak MN, Azmi AS, et al. G12C game of thrones, which direct KRAS inhibitor will claim the iron throne? *Cancer Treat Rev.* (2020) 84:101974. doi: 10.1016/j.ctrv.2020.101974

24. Mustachio LM, Chelariu-Raicu A, Szekvolgyi L, Roszik J. Targeting KRAS in cancer: promising therapeutic strategies. *Cancers.* (2021) 13:1204. doi: 10.3390/cancers13061204

25. Conroy M, Cowzer D, Kolch W, Duffy AG. Emerging RAS-directed therapies for cancer. *Cancer Drug Resist.* (2021) 4:543–58. doi: 10.20517/cdr.2021.07

26. Skoulidis F, Li BT, Dy GK, Price TJ, Falchook GS, Wolf J, et al. Sotorasib for lung cancers with KRAS pG12C mutation. *N Engl J Med.* (2021) 384:2371–81. doi: 10.1056/NEJMoa2103695

27. Hyun S, Shin D. Small-molecule inhibitors and degraders targeting KRAS-driven cancers. *Int J Mol Sci.* (2021) 22:12142. doi: 10.3390/ijms222212142

28. Strickler JH, Satake H, George TJ, Yaeger R, Hollebecque A, Garrido-Laguna I, et al. Sotorasib in KRAS pG12C-mutated advanced pancreatic cancer. *N Engl J Med.* (2023) 388:33–43. doi: 10.1056/NEJMoa2208470

29. Lanman BA, Allen JR, Allen JG, Amegadzie AK, Ashton KS, Booker SK, et al. Discovery of a covalent inhibitor of KRAS(G12C) (AMG 510) for the treatment of solid tumors. *J Med Chem.* (2020) 63:52–65. doi: 10.1021/acs.jmedchem.9b01180

30. Jänne PA, Riely GJ, Gadgeel SM, Heist RS, Ou S-HI, Pacheco JM, et al. Adagrasib in non-small-cell lung cancer harboring a KRAS(G12C) mutation. *N Engl J Med.* (2022) 387:120–31. doi: 10.1056/NEJMoa2204619

31. Tsai YS, Woodcock MG, Azam SH, Thorne LB, Kanchi KL, Parker JS, et al. Rapid idiosyncratic mechanisms of clinical resistance to KRAS G12C inhibition. *J Clin Invest.* (2022) 132:e155523. doi: 10.1172/JCI155523

32. Begum P, Goldin RD, Possamai LA, Popat S. Severe immune checkpoint inhibitor hepatitis in KRAS G12C-mutant NSCLC potentially triggered by sotorasib: case report. *JTO Clin Res Rep.* (2021) 2:100213. doi: 10.1016/j.jtocrr.2021.100213

33. Liu J, Kang R, Tang D. The KRAS-G12C inhibitor: activity and resistance. *Cancer Gene Ther.* (2022) 29:875–8. doi: 10.1038/s41417-021-00383-9

34. Chan C-H, Chiou L-W, Lee T-Y, Liu Y-R, Hsieh T-H, Yang C-Y, et al. and PI3K pathway activation confers resistance to KRAS(G12C) inhibitor sotorasib. *Br J Cancer.* (2023) 128:148–59. doi: 10.1038/s41416-022-02032-w

35. Liao Y, Smyth GK, Shi W. featureCounts: an efficient general purpose program for assigning sequence reads to genomic features. *Bioinformatics.* (2014) 30:923–30. doi: 10.1093/bioinformatics/btt656

36. Robinson MD, McCarthy DJ, Smyth GK. edgeR: a Bioconductor package for differential expression analysis of digital gene expression data. *Bioinformatics.* (2010) 26:139–40. doi: 10.1093/bioinformatics/btp616

37. Robinson MD, Oshlack A. A scaling normalization method for differential expression analysis of RNA-seq data. *Genome Biol.* (2010) 11:R25. doi: 10.1186/gb-2010-11-3-r25

38. Lun ATL, Chen Y, Smyth GK. It's DE-licious: a recipe for differential expression analyses of RNA-seq experiments using quasi-likelihood methods in edgeR. *Methods Mol Biol.* (2016) 1418:391–416. doi: 10.1007/978-1-4939-3578-9_19

39. Ritchie ME, Phipson B, Wu D, Hu Y, Law CW, Shi W, et al. limma powers differential expression analyses for RNA-sequencing and microarray studies. *Nucleic Acids Res.* (2015) 43:e47. doi: 10.1093/nar/gkv007

40. Law CW, Chen Y, Shi W, Smyth GK. voom: Precision weights unlock linear model analysis tools for RNA-seq read counts. *Genome Biol.* (2014) 15:R29. doi: 10.1186/gb-2014-15-2-r29

41. Law CW, Alhamdoosh M, Su S, Dong X, Tian L, Smyth GK, Ritchie ME. RNA-seq analysis is easy as 1-2-3 with limma, Glimma and edgeR. *F1000Research.* (2016) 5. doi: 10.12688/f1000research.9005.1

42. McCarthy DJ, Smyth GK. Testing significance relative to a fold-change threshold is a TREAT. *Bioinformatics.* (2009) 25:765–71. doi: 10.1093/bioinformatics/btp053

43. Tumminello M, Bertolazzi G, Sottile G, Sciaraffa N, Arancio W, Coronnello C, et al. Multivariate statistical test for differential expression analysis. *Sci Rep.* (2022) 12:8265. doi: 10.1038/s41598-022-12246-w

44. Vaes E, Khan M, Mombaerts P. Statistical analysis of differential gene expression relative to a fold change threshold on NanoString data of mouse odorant receptor genes. *BMC Bioinformat.* (2014) 15:39. doi: 10.1186/1471-2105-15-39

45. Szklarczyk D, Gable AL, Nastou KC, Lyon D, Kirsch R, Pyysalo S, et al. The STRING database in 2021: customizable protein-protein networks, and functional characterization of user-uploaded gene/measurement sets. *Nucleic Acids Res.* (2021) 49:D605–12. doi: 10.1093/nar/gkaa1074

46. Shannon P, Markiel A, Ozier O, Baliga NS, Wang JT, Ramage D, et al. Cytoscape: a software environment for integrated models of biomolecular interaction networks. *Genome Res.* (2003) 13:2498–504. doi: 10.1101/gr.12 39303

47. Wu T, Hu E, Xu S, Chen M, Guo P, Dai Z, et al. et al. clusterProfiler 40: A universal enrichment tool for interpreting omics data. *Innovation.* (2021) 2:100141. doi: 10.1016/j.xinn.2021.100141

48. Nagy Á, Munkácsy G, Gyorffy B. Pancancer survival analysis of cancer hallmark genes. *Sci Rep.* (2021) 11:6047. doi: 10.1038/s41598-021-8 4787-5

49. Yu L, Kim HT, Kasar S, Benien P, Du W, Hoang K, et al. Survival of Del17p CLL depends on genomic complexity and somatic mutation. *Clin cancer Res.* (2017) 23:735–45. doi: 10.1158/1078-0432.CCR-16-0594

50. Lánczky A, Gyorffy B. Web-based survival analysis tool tailored for medical research (KMplot): development and implementation. *J Med Internet Res.* (2021) 23:e27633. doi: 10.2196/27633

51. Vasta JD, Peacock DM, Zheng Q, Walker JA, Zhang Z, Zimprich CA, et al. KRAS is vulnerable to reversible switch-II pocket engagement in cells. *Nat Chem Biol.* (2022) 18:596–604. doi: 10.1038/s41589-022-00985-w

52. Parikh K, Banna G, Liu S V, Friedlaender A, Desai A, Subbiah V, et al. Drugging KRAS: current perspectives and state-of-art review. *J Hematol Oncol.* (2022) 15:152. doi: 10.1186/s13045-022-01375-4

53. Indini A, Rijavec E, Ghidini M, Cortellini A, Grossi F. Targeting KRAS in solid tumors: current challenges and future opportunities of novel KRAS inhibitors. *Pharmaceutics.* (2021) 13:653. doi: 10.3390/pharmaceutics13050653

54. Yang A, Li M, Fang M. The research progress of direct KRAS G12C mutation inhibitors. *Pathol Oncol Res.* (2021) 27:631095. doi: 10.3389/pore.2021.631095

55. Kwan AK, Piazza GA, Keeton AB, Leite CA. The path to the clinic: a comprehensive review on direct KRAS(G12C) inhibitors. *J Exp Clin Cancer Res.* (2022) 41:27. doi: 10.1186/s13046-021-02225-w

56. Tanaka N, Lin JJ Li C, Ryan MB, Zhang J, Kiedrowski LA, Michel AG, et al. Clinical acquired resistance to KRAS(G12C) inhibition through a novel KRAS switch-II pocket mutation and polyclonal alterations converging on RAS-MAPK reactivation. *Cancer Discov.* (2021) 11:1913–22. doi: 10.1158/2159-8290.CD-21-0365

57. Awad MM, Liu S, Rybkin II, Arbour KC, Dilly J, Zhu VW, et al. Acquired resistance to KRAS(G12C) inhibition in cancer. *N Engl J Med.* (2021) 384:2382–93. doi: 10.1056/NEJMoa2105281

58. Maharjan M, Tanvir RB, Chowdhury K, Duan W, Mondal AM. Computational identification of biomarker genes for lung cancer considering treatment and non-treatment studies. *BMC Bioinformat.* (2020) 21:218. doi: 10.1186/s12859-020-3524-8

59. Elhamamsy AR, Metge BJ, Alsheikh HA, Shevde LA, Samant RS. Ribosome biogenesis: a central player in cancer metastasis and therapeutic resistance. *Cancer Res.* (2022) 82:2344–53. doi: 10.1158/0008-5472.CAN-21-4087

60. Kang J, Brajanovski N, Chan KT, Xuan J, Pearson RB, Sanij E. Ribosomal proteins and human diseases: molecular mechanisms and targeted therapy. *Signal Transduct Target Ther.* (2021) 6:323. doi: 10.1038/s41392-021-00728-8

61. Yan T-T, Fu X-L, Li J, Bian Y-N, Liu DJ, Hua R, et al. Downregulation of RPL15 may predict poor survival and associate with tumor progression in pancreatic ductal adenocarcinoma. *Oncotarget.* (2015) 6:37028–42. doi: 10.18632/oncotarget.5939

62. Daftuar L, Zhu Y, Jacq X, Prives C. Ribosomal proteins RPL37, RPS15 and RPS20 regulate the Mdm2-p53-MdmX network. *PLoS ONE.* (2013) 8:e68667. doi: 10.1371/journal.pone.0068667

63. Yadavilli S, Mayo LD, Higgins M, Lain S, Hegde V, Deutsch WA. Ribosomal protein S3: a multi-functional protein that interacts with both p53 and MDM2 through its KH domain. *DNA Repair.* (2009) 8:1215–24. doi: 10.1016/j.dnarep.2009.07.003

64. Li Y, Zhou Y, Li B, Chen F, Shen W, Lu Y, et al. WDR74 modulates melanoma tumorigenesis and metastasis through the RPL5-MDM2-p53 pathway. *Oncogene.* (2020) 39:2741–55. doi: 10.1038/s41388-020-1179-6

65. Li C, Ge M, Yin Y, Luo M, Chen D. Silencing expression of ribosomal protein L26 and L29 by RNA interfering inhibits proliferation of human pancreatic cancer PANC-1 cells. *Mol Cell Biochem.* (2012) 370:127–39. doi: 10.1007/s11010-012-1404-x

66. El Khoury W, Nasr Z. Deregulation of ribosomal proteins in human cancers. *Biosci Rep.* (2021) 41. doi: 10.1042/BSR20211577

67. Alam E, Maaliki L, Nasr Z. Ribosomal protein S3 selectively affects colon cancer growth by modulating the levels of p53 and lactate dehydrogenase. *Mol Biol Rep.* (2020) 47:6083–90. doi: 10.1007/s11033-020-05683-1

68. Yang HJ, Youn H, Seong KM, Jin Y-W, Kim J, Youn B. Phosphorylation of ribosomal protein S3 and antiapoptotic TRAF2 protein mediates radioresistance in non-small cell lung cancer cells. *J Biol Chem.* (2013) 288:2965–75. doi: 10.1074/jbc.M112.385989

69. Yao Y-X, Xu B-H, Zhang Y. CX-3543 promotes cell apoptosis through downregulation of CCAT1 in colon cancer cells. *Biomed Res Int.* (2018) 2018:9701957. doi: 10.1155/2018/9701957

70. Makhale A, Nanayakkara D, Raninga P, Khanna KK, Kalimutho M. CX-5461 enhances the efficacy of APR-246 via induction of DNA damage and replication stress in triple-negative breast cancer. *Int J Mol Sci.* (2021) 22:5782. doi: 10.3390/ijms22115782

71. Hilton J, Gelmon K, Bedard PL, Tu D, Xu H, Tinker A V, et al. Results of the phase I CCTG IND.231 trial of CX-5461 in patients with advanced solid tumors enriched for DNA-repair deficiencies. *Nat Commun.* (2022) 13:3607. doi: 10.1038/s41467-022-31199-2

72. Sun M-Y, Xu B, Wu Q-X, Chen W-L, Cai S, Zhang H, et al. Cisplatin-Resistant gastric cancer cells promote the chemoresistance of cisplatin-sensitive cells via the exosomal RPS3-mediated PI3K-Akt-Cofilin-1 signaling axis. *Front cell Dev Biol.* (2021) 9:618899. doi: 10.3389/fcell.2021.618899

73. Wang T, Jin C, Yang P, Chen Z, Ji J, Sun Q, et al. UBE2J1 inhibits colorectal cancer progression by promoting ubiquitination and degradation of RPS3. *Oncogene.* (2023) 42:651–64. doi: 10.1038/s41388-022-02581-7

Chemico-Biological Interactions 357 (2022) 109876

Contents lists available at ScienceDirect

Chemico-Biological Interactions

journal homepage: www.elsevier.com/locate/chembioint

Research paper

Synthesis, in vitro and structural aspects of cap substituted Suberoylanilide hydroxamic acid analogs as potential inducers of apoptosis in Glioblastoma cancer cells *via* HDAC /microRNA regulation

Janaki Ramaiah Mekala [a,b,1,*], Prasanna Srinivasan Ramalingam [a,1], Sivagami Mathavan [c], Rajesh B.R.D. Yamajala [c], Nageswara Rao Moparthi [d], Rohil Kumar Kurappalli [a], Rajasekhar Reddy Manyam [d]

[a] Functional Genomics and Disease Biology Laboratory, School of Chemical and Biotechnology, SASTRA Deemed University, Thanjavur, 613401, Tamil Nadu, India
[b] Department of Biotechnology, Koneru Lakshmaiah Education Foundation, Green Fields, Vaddeswaram, Guntur, India
[c] Organic Synthesis and Catalysis Laboratory, School of Chemical and Biotechnology, SASTRA Deemed University, Thanjavur, 613401, Tamil Nadu, India
[d] Department of Computer Science and Engineering, Koneru Lakshmaiah Education Foundation, Green Fields, Vaddeswaram, Guntur, India

ARTICLE INFO

Keywords:
HDAC
Glioblastoma
HDAC-8
MicroRNA
SAHA analog
Rictor

ABSTRACT

Glioblastoma multiforme (GBM) is a heterogeneous, aggressive brain cancer characterized by chemo-resistance and cancer stemness. Histone deacetylases (HDACs) are a group of enzymes that regulate chromatin epigenetics which were in turn found to be controlled by microRNAs (miRs). The drug employed in chemotherapy for the treatment of GBM is Temozolomide (TMZ). Unfortunately, many GBM patients exhibit chemo-resistance to this drug. Here we have synthesized various Suberoyl anilide hydroxamic acid (SAHA) analogs with many substitutions at the cap site majority of which not yet studied. These SAHA analogs have exhibited profound cytotoxicity at 2 μM, and 4 μM concentrations in GBM cancer cell line U87MG, and 1 μM, and 2 μM concentrations in breast cancer cell line MCF-7. Surprisingly, these analogs have exhibited cytotoxic effects in chronic lymphoid leukemia cells (Raji) at 64 μM, and 128 μM concentrations due to mutated p53. Among all the synthesized analogs 3-Chloro-SAHA, 3-Chloro-4-fluoro SAHA have exhibited effective cytotoxicity in all cancer cells. These potent analogs inhibited HDAC-8 enzyme activity by 2-folds in U87MG, and MCF-7 cell lines and 7-folds decrease in HDAC-8 activity was observed in Raji cell line. These analogs decreased the expression of HDAC-2, HDAC-3 genes and enhanced the expression of p53 tumor suppressor. Interestingly, these compounds decreased the expression of Rictor, the main component of the mTORC2 complex involved cancer cell metabolism. Furthermore, these molecules have decreased oncogenic microRNA expression such as miR-21 and enhanced the expression of tumor suppressor microRNAs such as miR-143. The HDAC binding ability of these molecules was highly significant and have exhibited the ability to cross blood-brain barrier (BBB), and followed the Lipinski rule of five. Thus, these molecules need to be taken up further to clinics for better therapy against GBM either singly or combination therapy.

1. Introduction

The acetylation and deacetylation of histones regulate chromatin epigenetics, as well as gene expression, and was mediated by two groups of enzymes such as histone acetyl transferases (HATs), and histone deacetylases (HDACs). The HDAC enzymes catalyze the removal of the acetyl group from the lysine residues of the histone tail and induce the non-permissive chromatin state and suppress the transcription of genes [1]. Thus, inhibition of HDACs by HDAC inhibitor (HDACi) results in changes in gene expressions at tumor suppressor gene-specific loci leading to the inhibition in the cancer cell growth, and proliferation. Generally, HDACs are classified into class I (HDAC-1, HDAC-2, HDAC-3, and HDAC-8), class II HDACs are further classified into class IIa (HDAC-4, HDAC-5, HDAC-7, and HDAC-9), and class IIb (HDAC-6 and

* Corresponding author. Department of Biotechnology, Koneru Lakshmaiah Education Foundation, Green fields, Vaddeswaram, Guntur, 522302, India.
E-mail address: janakiramaiah@kluniversity.in (J.R. Mekala).
[1] Equal first.

https://doi.org/10.1016/j.cbi.2022.109876
Received 12 December 2021; Received in revised form 4 February 2022; Accepted 28 February 2022
Available online 10 March 2022

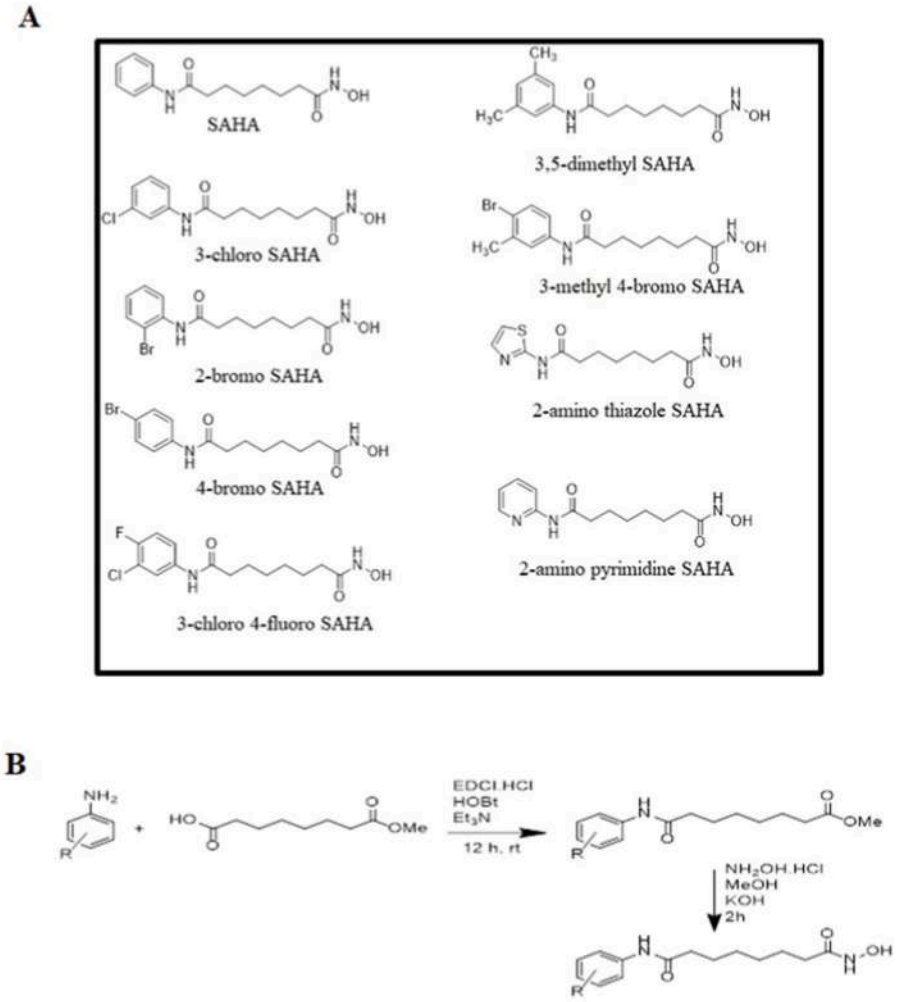

Fig. 1. a. Various SAHA analogs were synthesized in the study. The SAHA analogs that are cap substituted such as 3-Chloro, 3-Chloro-4-fluoro, 2-Bomo, 4- Bromo, 3,5-dimethyl SAHA, 3-methyl-4-bromoSAHA, 2-aminothiazole SAHA, 2-amino pyrimidine SAHA were studied. Fig. 1b. Scheme of synthesis of SAHA analogs.

HDAC-10), class III (Sirtuins 1,2,3,4,5,6 and 7) and class IV (HDAC-11) [2]. HDACi are broadly classified into Hydroxamic acids, Aliphatic acids, Sirtuin inhibitors, Benzamides and, Cyclic depsipeptides/tetrapeptides [3].

The HDAC inhibitors such as Suberoyl anilide hydroxamic acid (SAHA), Belinostat (PXD-101), Fimepinostat (CUDC-907), Entinostat (MS-275, NSC706995), Panobinostat (LBH589), ACY-1215, Valproic acid (VPA), and Butyric acid have revealed anti-cancer potential against lymphoma, multiple myelomas, leukemia, breast cancer, colon cancer, lung cancer, and renal cell carcinoma [3,4]. The Food and Drug Administration (FDA) approved HDAC inhibitors include Vorinostat (SAHA), Belinostat, Panobinostat, and Romidepsin for the treatment of T-cell lymphomas that include cutaneous T-cell lymphoma, and peripheral T-cell lymphoma. Apart from this, various HDAC inhibitors such as Trichostatin A (TSA), Givinostat, Quisinostat, Practinostat, Valproic acid, Entinostat, and Nicotinamide were in clinical trials against myeloma and solid tumors [5].The Vorinostat/suberoylanilide hydroxamic acid (SAHA) have the potent ability to increase the intracellular ROS levels; induces cell-cycle arrest, inhibits HDAC protein levels, induces apoptosis by the upregulation and downregulation of pro-apoptotic and anti-apoptotic proteins respectively in various cancers [6,7].

Glioblastoma (GBM) is a primary malignant brain tumor wherein therapeutic options are very limited. The most important chemotherapeutic drug used for the treatment of GBM includes Temozolomide (TMZ). Many GBM patients have exhibited resistance to Temozolomide [8]. Recent studies reported that the HDACi such as Suberoylanilide hydroxamic acid (SAHA) induce autophagy as well as inhibit cell proliferation in glioblastoma effectively when used as combination with chloroquine (CQ)/alone [9]. SAHA plays a vital role in cancer epigenetics by inhibiting the HDAC protein levels, enhance histone acetylation level and thereby upregulate p21WAF1 and downregulate Vascular endothelial growth factor (VEGF), Interestingly, SAHA treatment hyperacetylates heat shock protein 90 (HSP90) thereby downregulation Raf-1 kinase and ultimately lead to cell-cycle arrest and apoptosis in cancer cells [10].

A novel HDAC6 selective inhibitor JOC1 has exhibited high cytotoxicity, induce apoptosis, suppress glioblastoma stem cells (GSC) proliferation [11]. [12] have demonstrated that the Mocetinostat HDAC-1/2, 3 selective inhibitor) and MC2129 (uracil-based hydroxy amides) new class I/IIb selective HDAC inhibitors induce cell-cycle arrest, and inhibit proliferative activity without affecting astrocyte survival and were found to be more potent than FDA approved SAHA.

Valproic acid, a Class I and IIa HDACi suppress the nuclear factor kappa B (NF-kB), penetrates the blood-brain barrier (BBB), and inhibits HDAC activity, induces apoptosis, and is mostly used to relieving seizures by antiepileptic activity in GBM treatment [13]. Entinostat, a class I HDAC inhibitor was reported to cross the BBB, increases intracellular ROS by damaging the mitochondrial membrane, induce apoptosis, upregulate p21, and thus induces cell cycle arrest at G0/G1 phase in

GBM [14].

Importantly, to treat glioblastoma the drug molecules should cross the blood-brain barrier (BBB) which is comparatively easy for small molecules like SAHA, rather than the larger molecules that could not penetrate BBB to reach the glioblastoma tumor environment [15]. Although, SAHA inhibits the HDACs and induces cell cycle arrest, and cause effective apoptosis in various GBM cancer cell lines such as U87-MG, U251-MG. U373-MG [11]. So, synthesizing various SAHA analogs and studying their therapeutic potential and BBB penetration potential may shed light on the new drug discovery for the treatment of glioblastoma in the future.

Altered expression/activity of histone deacetylases (HDACs) were found to be associated with poor prognosis. Inhibition of HDAC activity using histone deacetylase inhibitors (HDACi) has been a promising therapy against GBM [16]. MicroRNAs (miRNAs) are small non-coding RNAs that bind to the 3′-untranslated region (3′-UTR) of mRNA and regulate the gene expression. MicroRNAs were involved in several processes of cancer cells such as proliferation, and apoptosis. Studies have also indicated that microRNAs are an integral part of epigenetic machinery [17–21] and several epigenetic modifiers such as histone deacetylase proteins were in turn found to regulate the microRNA expression. In addition, miRNAs regulate the chromatin architecture which is regulated by epigenetic proteins. Thus, miRNAs and epigenetic proteins such as HDACs have a crucial regulatory role on gene expression [22].

Like in any other cancer in GBM cancer also few microRNAs were found to be upregulated and are involved in cancer progression known as OncomiRs while certain other microRNAs were found to be down-regulated and were known as tumor suppressor miRs. MiR-21 was found to be upregulated in various grades of astrocytic tumors and was known to inhibit tumor suppressor genes [23]. On other hand, miR-15b inhibits cancer cell proliferation by targeting the insulin-like growth factor (IGF1R), thus functioning as tumor suppressor [24]. Compounds modulating miR-15b was a useful therapeutic strategy against GBM cancer.

2. Materials and methods

2.1. Chemistry: synthesis methodology of SAHA analogs

For SAHA derivative, suberic acid monomethyl ester was attached to aniline by amide coupling using EDCI and HOBT. The resulting suberanilic acid methyl ester was hydrolyzed with hydroxylamine hydrochloride and KOH to get the suberoylanilide hydroxamic acid (SAHA). Similarly, the SAHA derivatives were synthesized by reacting various substituted anilines by following the above-described procedure (Fig. 1a). The detailed procedure for the synthesis of SAHA was given in Supplementary file 6.

All of the SAHA analogs were produced in pure form and were characterized by 1H NMR spectra. 1H NMR was recorded on a Bruker AVANCE III 400 MHz NMR at 400.

2.2. Cell culture

The cell lines U87MG, Raji, and MCF-7 were cultured in Dulbecco's Modified Eagles Medium (DMEM), and RPMI-1640 medium supplemented with 2 mM L-glutamine (Gibco), 10% FBS (HiMedia Laboratories, USA), with antimycotic antibiotic solution (HiMedia Laboratories, USA) and maintained at 37 °C in a 5% CO_2 incubator. HCN2 (Normal cells) were maintained DMEM medium supplemented with 2 mM -L-Glutamine.

2.3. MTT assay

The cytotoxic potential of anti-cancer compounds was determined by the MTT cytotoxicity assay, in which the yellow color MTT dye is reduced to insoluble purple color formazan crystals which can be quantified at optical density (OD)570 nm. 1x10^5density of U87MG, Raji, and MCF-7 cells were seeded in a 96-well plate and incubated for 24 h, followed by the treatment of SAHA, and novel SAHA analogs at various concentrations ranging from 1 to 4 μM (MCF-7), 16–128 μM (for Raji), 2–4 μM (U87MG) and normal cells HCN2 was incubated for 24 h. Then 50 μL MTT dye was added and plates were further incubated at 37 °C for 2 h and solubilized in the solubilizing buffer and the absorbance was measured at 570 nm in Multimode varioscan (Thermo Scientifics).

2.4. ROS detection

The intracellular ROS levels was determined using H_2DCFDA probe method according to the manufacture's protocol. The H2DCFDA (2′,7′-Dichlorodihydrofluorescein diacetate) is a colourless non-fluorescent ROS probe, hydrolyzed into H2DCF by the esterases inside the cell that converts acid groups into alcohol groups. Then the H2DCF is oxidized by H_2O_2 in the presence of Fe^{2+} ferrous ion, into a green fluorescent product called DCF (2′,7′-dichlorofluorescein). The U87MG cells, MCF-7, and Raji cells were seeded in a 25 mm^2 culture flask and incubated for 24 h at 5% CO_2, followed by the treatment of SAHA and potential novel SAHA analogs and further incubated for 24 h. Then the cells were briefly trypsinized and centrifuged at 4000 rpm for 5 min, and 50 μL of H2DCFDA dye was added to the cell pellet and incubated for 30 min at 37 °C in dark. Then the fluorescence was quantified using 470 nm excitation spectra and 530 nm emission spectra in Multimode Varioscan (Thermo Scientifics).

2.5. HDAC-8 activity assay

The HDAC-8 activity was determined using HDAC8 Activity Assay Kit (Fluorometric) (ab156069) according to the manufacture's protocol. The protein substrate acetylated at lysine residue was labeled with a chromophore MCA (7-Amino-4-methylcoumarin), that is deacetylated by the HDAC-8 and further cleaved by the peptidases into peptide and blue fluorescent AMC (C-terminal 7-amino-4-methylcoumarin) was quantified. The U87MG, Raji, MCF-7 cells were seeded in a 25 mm^2 culture flask and incubated for 24 h at 5% CO_2, followed by the treatment of SAHA and novel SAHA analogs and further incubated for 24 h. Then the cells were briefly trypsinized and centrifuged at 4000 rpm for 5 min, and 0.2 mM Fluoro-substrate peptide, and developer were added and were further incubated at 37 °C for 1 h in dark. The fluorescence was quantified using 350 nm excitation spectra and 440 nm emission spectra in Multimode varioscan (Thermo Scientifics).

2.6. Colony formation assay

The 1×10^3 U87MG cells were seeded in each well of the 6-well plate and allowed them to form colonies for a week time. Then treat the wells with novel potent SAHA analogs for 48h. The colonies were counted.

2.7. Reverse transcription polymerase chain reaction (RT-PCR) analysis

The total RNA was isolated from control, SAHA and novel SAHA analogs treated cells by Trizol method (Invitrogen). Then the first strand cDNA is synthesized by superscript III (SSIII) reverse transcriptase (Invitrogen) using Oligo(dT)s as primers. The RT-PCR analysis was performed with specific gene primers for GAPDH, HDAC1, HDAC2, HDAC3, HDAC8, Drosha, Dicer, Rictor in the Bio-Rad Thermal cycler with their respective reaction condition [21]. Then the polymerase chain reaction (PCR) products were run in 2% agarose gel and pictures were taken gel doc system (BIO-RAD). Then the band intensities were quantified using image J software.

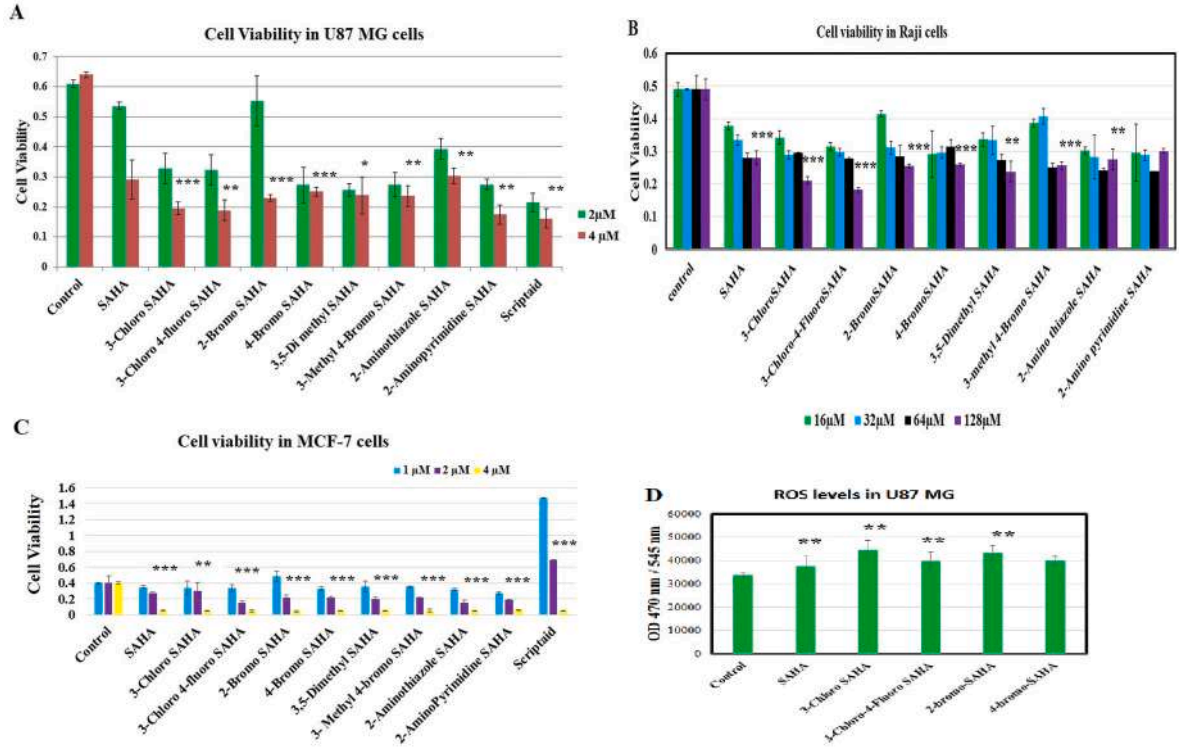

Fig. 2. Effect of SAHA analogs on cancer cell viability and effect on production of reactive oxygen species (ROS) (A). The U87MG cells were treated with SAHA analogs such as 3-ChloroSAHA, 3-Chloro-4-fluoroSAHA, 2-BromoSAHA, 4-BromoSAHA, 3,5-dimethyl SAHA, 3-methyl-4-bromoSAHA, 2-aminothiazole SAHA, 2-aminopyrimidine SAHA at concentrations of 2 μM, and 4 μM for 24h. This is followed by MTT assay. The OD at 570 nm was measured. The cells which exhibit less OD have less viability. Control indicates cells treated with DMSO. Here the parent molecule SAHA was also used for comparative study. **(B).** The Raji cells were treated with SAHA analogs such as 3-ChloroSAHA, 3-Chloro-4-fluoroSAHA, 2-BromoSAHA, 4-BromoSAHA, 3,5-dimethyl SAHA, 3-methyl-4-bromoSAHA, 2-aminothiazole SAHA, 2-aminopyrimidine SAHA at concentrations of 2 μM, and 4 μM for 24h. This is followed by MTT assay. The OD at 570 nm was measured. The cells which exhibit less OD have less viability. Control indicates cells treated with DMSO. Here the parent molecule SAHA was also used for comparative study **(C).** The MCF-7 breast cancer cells were treated with SAHA analogs such as 3-ChloroSAHA, 3-Chloro-4-fluoroSAHA, 2-BromoSAHA, 4-BromoSAHA, 3,5-dimethyl SAHA, 3-methyl-4-bromoSAHA, 2-aminothiazole SAHA, 2-aminopyrimidine SAHA at concentrations of 2 μM, and 4 μM for 24h. This is followed by MTT assay. The OD at 570 nm was measured. The cells which exhibit less OD have less viability. Control indicates cells treated with DMSO. Here the parent molecule SAHA was also used for comparative study. **(D).** The U87MG cells were seeded at a density of 10000 cells/well and incubated for 24h. This is followed by treatment with various SAHA analogs such as 3-chloro SAHA, 3-chloro-4-fluoro SAHA, 2-bromo SAHA, 4-bromo SAHA at 4 μM for 24h. The OD at 470/545 nm was measured. The optical density (OD) is indicative of ROS generation. Control: U87MG cells without any treatment.

2.8. Annexin V-FITC/PI staining

The apoptosis induction in control and drug treated cells was determined by Annexin V-FITC staining Kit (Abcam, UK) according to the manufacture's protocol. Apoptosis is a molecular event in which a cell undergoes a programmed cell death *via* phospholipid bilayer disruption. Phosphatidylserine (PS), a negatively charged phospholipid binds with Ca^{2+} ions and faced towards the cytoplasmic face in a normal cell. During early apoptosis, it traversed by flippase towards the exoplasmic side, where the Annexin (Ca^{2+} binding protein) directly binds to PS and is visualized as green color. The U87MG cells were cultured in a 6 well plate of the area and incubated for 24 h at 5% CO_2, followed by the treatment of SAHA and novel SAHA analogs and further incubated for 24 h. Then the cells were briefly trypsinized and spun at 4000 rpm for 5 min, and a binding buffer containing 5 μL Annexin V and 10 μl PI was added to the cells and incubated at 37 °C for 15 min. Then the cells were visualized at wavelength of 550 nm excitation spectra and emission spectra at a wave length of 620 nm in the 40X magnification of fluorescent microscope (Eclipse Ni–U, Nikon, Japan).

2.9. MicroRNA expression study

The Total RNA was isolated from the control and the compound-treated U87MG cells. The cDNA prepared was subjected microRNA expression study and followed the manufacturer's recommendations (System biosciences) [21].

2.10. Scratch assay

A wound healing assay was conducted to understand the migration ability of U87MG cells Around 10,000 Cells were seeded in 6-well plates and allow the cells to attain 90% confluency. Further scratch will be made (i.e. artificial wounds) by using a 200-μl pipette tip. After 24h, the wound closure was examined and imaged under a microscope and migration was quantified (Supplementary Fig. 5).

2.11. Statistical analysis

The graph graph-pad prism V.8 was used for statistical analysis and the data were represented as Mean ± SD. One-way analysis of variance followed by Tukey's test/posthoc test was performed to determine the significant difference among the groups and multiple comparisons were followed. The values * denotes $p < 0.05$, ** denotes $p < 0.01$, *** denotes $p < 0.005$ and **** denotes $p < 0.001$.

3. Results and discussion

3.1. Effect of SAHA analogs on cell viability

The main drug employed for chemotherapy in GBM patients is

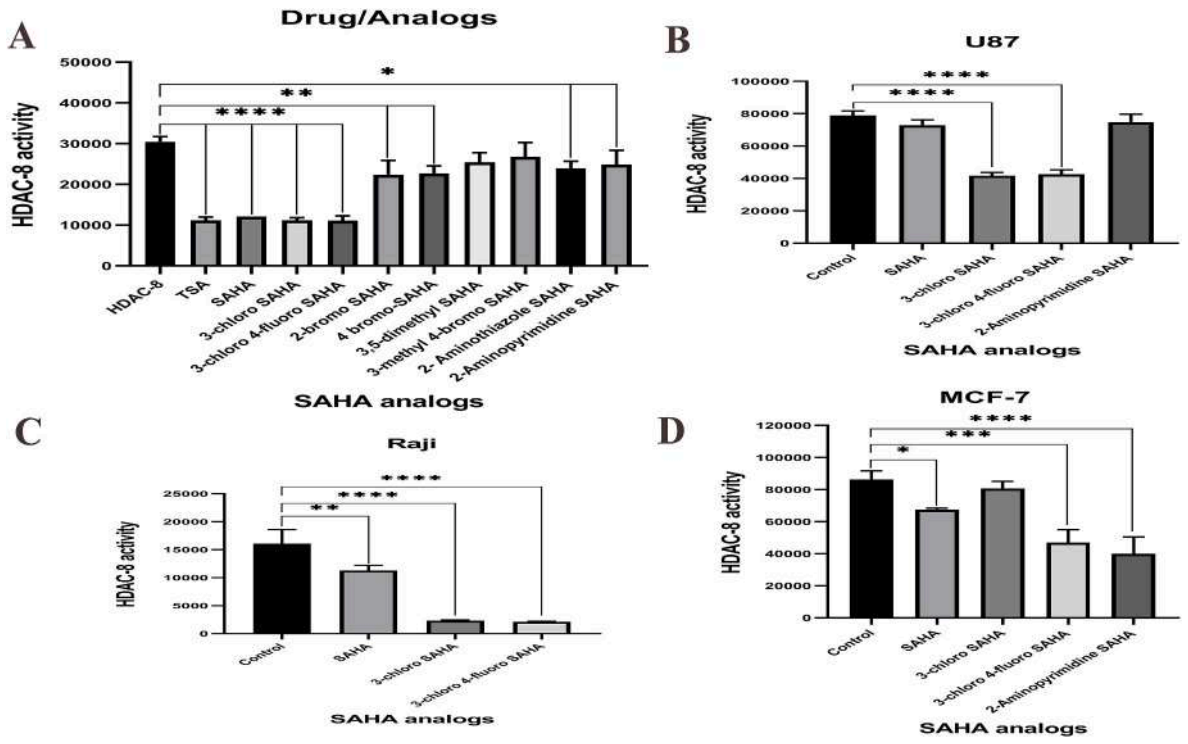

Fig. 3. Effect of SAHA analogs on HDAC-8 activity. **(A).** The SAHA analogs (compounds) were incubated HDAC-8 protein and was subjected to fluorometry. **(B).** Effect of SAHA analogs such 3-Chloro SAHA, 3-Chloro-4-fluoro SAHA, and 2-Amino pyrimidine SAHA on HDAC-8 activity in U87MG cells. **(C).** The effect of potent SAHA analogs on HDAC-8 activity in Raji (Chronic lymphoid leukemia cells). **(D).** Effect of SAHA analogs on HDAC-8 activity in MCF-7 breast cancer cells. Here the standard HDAC inhibitory molecules such as Trichostatin (TSA), and Suberoyl anilide hydroxamic acid (SAHA) were also employed for the comparative study. HDAC-8 or Control indicates the reaction in which compound or analog was not added.

Temozolomide. But many patients are exhibiting chemo-resistance due to its heterogeneous nature of GBM cancer and cancer stemness [25]. Thus, it is highly important to identify chemotherapeutic drugs that can induce effective apoptosis. In order to understand the effect of SAHA analogs on cell viability on cancer cells such as U87MG (GBM cancer) with 2 μM and 4 μM, Raji cells (CLL) with 16–128 μM, and MCF-7 (breast cancer) with 1–4 μM for 24h (Fig. 1a and b). The cell viability was measured by taking optical density (OD) at 570 nm. We have observed 3-Chloro SAHA, 3-Chloro-4-fluoro SAHA, and 2-aminopyrimidine SAHA have exhibited profound cytotoxic effects at 4 μM with GBM cancer cells. Raji cells which are chronic lymphoid cells have exhibited cytotoxicity at 128 μM when treated with 3-Chloro SAHA, 3-Chloro-4-fluoro SAHA. These SAHA analogs have exhibited profound cytotoxicity with breast cancer cells at 2 μM, and 4 μM concentrations. (Fig. 2a–c). Further, these analogs have not exhibited significant toxicity in normal HCN2 cells **(Supplementary file 4)** In addition, the GBM cancer cells treated with SAHA analogs were tested for their ability to induce Reactive oxygen generation (ROS). We have observed only GBM cancer cells have exhibited ROS production in U87MG cells. This indicates SAHA analogs with Chloro SAHA, 3-Chloro-4-fluoro SAHA were found to be effective cytotoxic (Fig. 2d).

3.2. Effect of SAHA analogs on histone deacetylase-8 activity

Studies have shown that inhibition of HDAC-8 was considered as an important aspect in understanding the therapeutic efficiency of chemotherapeutic drug. Here we have examined the HDAC-8 inhibitory property of these potent SAHA analogs in Glioblastoma (U87MG), chronic lymphoid leukemia (Raji), and breast cancer cells (MCF-7). We observed a 2-fold in decrease HDAC-8 activity in the U87MG and MCF-7 breast cancer cells treated with 3-Chloro SAHA, 3-Chloro-4-fluoro SAHA analogs. Surprisingly, in Raji (CLL) cells have showed the HDAC-8 inhibitory activity was up to 7-folds (Fig. 3). We have observed 3-Chloro-4-fluoro SAHA, 3-Chloro SAHA as potential HDAC-8 inhibitors when compared all the SAHA analogs tested (Fig. 3).

3.3. Effect of HDAC inhibitors on apoptosis

It was established fact that histone deacetylase inhibitors function as a potential inducer of cell-cycle arrest, and apoptosis in solid, and hematological malignancies [26]. Thus, we have examined the apoptotic induction ability of potent novel SAHA analogs in U87MG cells using Annexin-FITC labeling assay. Annexin V was found to be a calcium-binding protein that binds phosphatidylserine (PS). Here U87MG cells were treated with potent SAHA analogs (3-Chloro SAHA, and 3-Chloro-4-fluoro SAHA) at 4 μM concentration for 24h. We have observed increased apoptosis in U87MG cancer cells treated with potent SAHA analogs. This indicates the SAHA with 3-Chloro and 3-Chloro 4-fluoro substitutions at the cap site have a potent apoptotic inducing ability against GBM cancer cells (Fig. 4a). Similarly, these compounds have exhibited an inhibitory effect on cancer cell colony-forming ability as observed by crystal violet-based colony-forming assay, and also inhibited cancer cell migration by scratch assay (Fig. 4b; Supplementary file-5).

3.4. Effect of SAHA analogs on class I HDAC and rictor gene expression

Recent studies have identified various genetic, as well as epigenetic abnormalities involved in glioma pathogenesis and were found to be linked to cancer cell metabolism. Rictor is an important protein that regulates the mTORC2 activity and was found to be involved in the regulation of chromatin epigenetics and cancer cell proliferation [27]. To understand the effect of SAHA analogs on gene expression of various genes such as HDAC-1, HDAC-2, HDAC-3, and HDAC-8 as well as tumor suppressor genes p53, and PTEN, and Rictor. U87MG cells were treated with novel SAHA analogs for 24h. Gene expression study by reverse

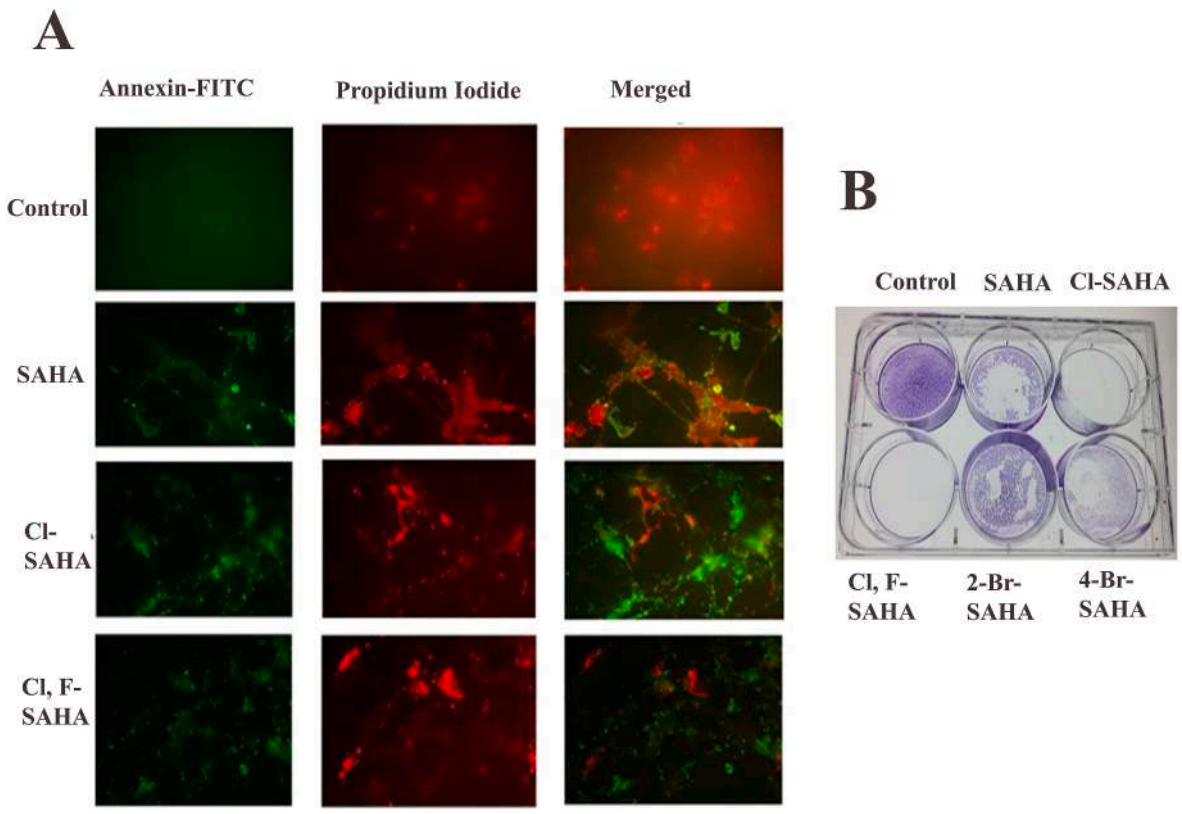

Fig. 4. (a). Effect of SAHA analogs in GBM cancer cell apoptosis. The U87MG cells were treated with SAHA, 3-ChloroSAHA, 3-Chloro 4-fluoroSAHA at 4 μM for 24h. Annexin-FITC was used stain to detect the apoptotic cells. The cells that undergo apoptosis was indicated by (green coloured cells). The nucleus was stained with propidium iodide (red). Control: U87MG cells without any treatment. **(b). Effect of SAHA analogs on colony forming ability.** The U87MG cells were allowed to form colonies and then these colonies were treated with SAHA analogs such as 3-ChloroSAHA, 3-Chloro 4-fluoroSAHA, 2-bromoSAHA, 4-BromoSAHA at 4 μM for 24h. The SAHA analogs such as 3-ChloroSAHA, 3-Choro-4-fluoro SAHA have exhibited reduction in colony forming ability of GBM cancer cells. Control: Control cells without any treatment. (For interpretation of the references to color in this figure legend, the reader is referred to the Web version of this article.)

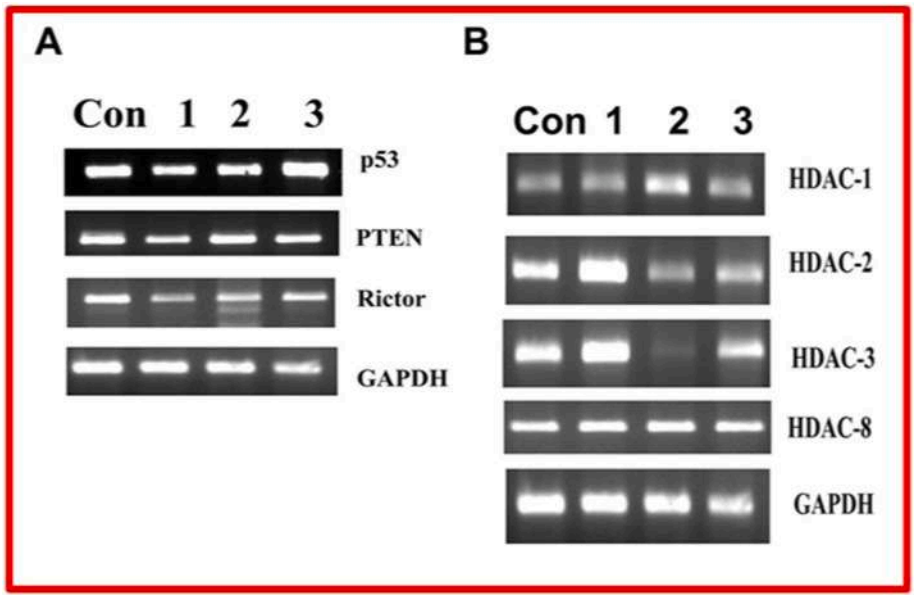

Fig. 5. Effect of SAHA analogs on Gene expression of tumor suppressors, RNA interference related genes, and Class I HDAC genes. The U87MG cells were treated with SAHA analogs at 4 μM concentration for 24h. The Total RNA isolated was reverse transcribed and was subjected to Reverse transcription PCR using primers against p53, PTEN, HDAC-1, HDAC-2, HDAC-3, and HDAC-8. The GAPDH used in the A and B is the same. C: Control cells without any treatment. 1: SAHA; 2 = 3-Chloro SAHA; 3 = 3 = Chloro-4-fluoro SAHA. GAPDH is same for all the gene expression studies carried out.

transcription-polymerase chain reaction (RT-PCR) has shown a decrease in expression of Rictor, HDAC-2, and HDAC-3. But the mRNA expression level of HDAC-1, and HDAC-8 remains the same (Fig. 5). Similarly, these analogs were tested for their ability to influence the gene expression of tumor suppressor genes such as p53, and PTEN that are involved in apoptosis. We have observed 3-Chloro-4-fluoro SAHA has exhibited enhanced p53 gene expression.

Table 1
Binding energies of SAHA and novel analogs against class I HDACs.

Class I HDAC's	Binding energies (Kcal/mol) of Drug/analogs								
	SAHA	A	B	C	D	E	F	G	H
HDAC1	−5.7	−5.6	−6	−5.4	−5.8	−6.2	−5.8	−5.9	−6.7
HDAC2	−6.4	−6	−6.1	−5.5	−6.3	−6.4	−6.0	−6.2	−7.3
HDAC3	−6	−5.9	−6	−5.4	−5.9	−6.4	−5.9	−5.8	−6.8
HDAC8	−5.8	−6.1	−5.9	−5.9	−6.1	−6.9	−6.2	−5.8	−6.6

SAHA= Suberoyl anilide hydroxamic acid, **A** = 3,5 Dimethyl SAHA; **B** = 3-Methyl-4-Bromo SAHA; **C**=Thiazole SAHA; **D** = Pyridine SAHA; **E** = 3-Chloro SAHA; **F** = 2-Bromo SAHA; **G** = 4-Bromo SAHA; **H** = 3-Chloro-4-Fluoro SAHA.

Table 2
Drug likeness properties of SAHA and its novel analogs.

Properties	Drug/analogs								
	SAHA	A	B	C	D	E	F	G	H
H-bond donor	3	3	3	3	3	3	3	3	3
H-bond acceptor	3	3	3	4	4	3	3	3	4
Molecular mass	264.32	292.3	357.2	271.3	265.3	298.7	343.2	343.2	316.7
LogP	1.92	2.57	3.02	1.2	1.29	2.38	2.52	2.4	2.87

Note: SAHA= Suberoyl anilide hydroxamic acid, **A** = 3,5 Dimethyl SAHA; **B** = 3-Methyl-4-Bromo SAHA; **C** = 2-Amino Thiazole SAHA; **D** = 2-Amino Pyrimidine SAHA; **E** = 3-Chloro SAHA; **F** = 2-Bromo SAHA; **G** = 4-Bromo SAHA; H = 3-Chloro-4-Fluoro SAHA.

Table 3
ADME properties of SAHA and its novel analogs.

Properties	Drug/analogs								
	SAHA	A	B	C	D	E	F	G	H
Lipophilicity	1.92	2.57	3.02	1.2	1.29	2.38	2.52	2.4	2.87
Hydrophilicity	−2.22	−2.67	−3.68	−1.86	−1.75	−2.65	−2.68	−2.97	−3.09
GI absorption	High	High	High	High	High	High	High	High	High
BBB permeability	Yes	No	No	No	No	Yes	No	No	Yes
Bioavailability	0.55	0.55	0.55	0.55	0.55	0.55	0.55	0.55	0.55
Synthetic accessibility	1.91	2.12	2.21	2.75	2.24	2.08	2.17	2.13	2.22

Note: SAHA= Suberoyl anilide hydroxamic acid, **A** = 3,5 Dimethyl SAHA; **B** = 3-Methyl-4-Bromo SAHA; **C** = 2-Amino Thiazole SAHA; **D** = 2-Amino Pyrimidine SAHA; E = 3-Chloro SAHA; **F** = 2-Bromo SAHA; **G** = 4-Bromo SAHA; **H**=3-Chloro-4-Fluoro SAHA.

3.5. Studies on interactions of class I HDACs with novel SAHA analogs

The three-dimensional docked complex of SAHA and its novel analogs with HDAC-1, HDAC-2, HDAC-3, and HDAC-8 were visualized in pymol and their bonding interactions were evaluated through Lig Plot + program. The binding energies of SAHA and all the novel SAHA analogs were given in (Table-1), and their drug-likeness and ADME properties were given in (Table 2 and 3) respectively. From the above results, we predicted that the 3-Chloro SAHA and 3-Chloro-4-fluoro SAHA have the potential to cross the blood-brain barrier, and has the potential to target glioblastoma. Furthermore, we also studied the bonding interactions of these two analogs along with SAHA as a standard, with Class I HDACs and their surrounding amino acid residues (Around 4 Å), Hydrogen bonds (H-bonds) with distance and hydrophobic interactions was given in detail in Table 4 and Table 5. The surface model, protein-ligand interactions, and the lig plot + model of the docked complexes of SAHA, 3-Chloro SAHA, and 3Chloro 4-Fluoro SAHA with the above proteins were shown in Supplementary File 2, Supplementary Fig. 3, & Fig. 6a–6d.

With HDAC-1, the SAHA, 3-ChloroSAHA, and 3-Chloro 4-Fluoro SAHA have exhibited a binding energy of −5.7 kcal/mol, −6.2 kcal/mol, and −6.7 kcal/mol. With HDAC-2, the SAHA, 3-Chloro SAHA, and 3-Chloro 4-Fluoro SAHA have shown binding energies of −6.4 kcal/mol, −6.4 kcal/mol, and −7.3 kcal/mol. With HDAC-3, SAHA, 3-Chloro SAHA, and 3-Chloro 4-Fluoro SAHA bind effectively with the binding energy of −6.0 kcal/mol, −6.4 kcal/mol, and −6.8 kcal/mol. With HDAC-8, the SAHA, 3-Chloro SAHA, and 3-Chloro 4-Fluoro SAHA have shown the binding energy of −5.8 kcal/mol, −6.9 kcal/mol, and −6.6 kcal/mol (Fig. 6).

3.6. Effect of SAHA analogs on microRNA expression

Glioblastoma relies on aerobic glycolysis, and sustained proliferation. During GBM pathogenesis dysregulation of microRNAs is involved in the regulation of the cancer cell metabolism, proliferation, invasion, and metastasis [21,26]. We have investigated the microRNA modulatory role of SAHA analogs on the expression of miR-143 that targets hexokinase (HK2), miR-15–3p, and miR-21 that participate in cancer cell proliferation in GBM. We have observed a decreased expression of oncogenic miRs such as miR-15–3p, and miR-21. And an increased expression of miR-143 cause tumor cell apoptosis (Fig. 7). No significant change in miR-17 in SAHA analogs treated U87MG cells.

4. Discussion

Histone deacetylases (HDACs) were known to regulate chromatin epigenetics, cell-cycle, cell migration, and involved various disease conditions such as cancer. Thus, HDAC inhibitors that inhibit HDAC gene or protein expression were considered as promising therapies against cancer. Suberoylanilide hydroxamic acid (SAHA) is the first approved histone deacetylase inhibitor (HDACi) approved by Food and Drug Administration (FDA). SAHA was found to inhibit class I, II, and IV HDACs [28,29]. Emerging studies have shown that SAHA can cross blood-brain barrier [30]. Studies on C4-benzyl SAHA displayed 520–1300 fold increase in selectivity for HDAC-6, and HDAC-8 than HDAC-1, HDAC-2, and HDAC-3 [31]. And C2-*n*-hexyl SAHA displayed sub-micromolar potency with 49-300-fold selectivity for HDAC6/HDAC8 than HDAC-1, HDAC-2, and HDAC-3 and were found to target

Table 4
H-Bond interactions of SAHA and novel analogs against class I HDACs.

Protein name	Drug/ analog	Surrounding amino acid residues (Around 4 Å)	Interacting hydrophobic residues
HDAC1	SAHA	ASP99, GLY149, PHE150, HIS178, GLU203, TYR204, PHE205, LEU271	ASP99, GLY149, PHE150, TYR204, LEU271
	3-Cl SAHA	TRY14, TYR54, ARG55, HIS57, LYS58, ALA59, GLU63, GLY115, VAL118, ALA119, VAL122, LYS123, GLN128	TRY14, TYR54, ARG55, LYS58, ALA59, GLY115, VAL118, ALA119, VAL122, LYS123
	3-Cl, 4-F SAHA	ASN95, VAL96, GLY97, GLU98, ASP99, CYS100, HIS141, SER148, GLY149, PHE150, HIS178, PHE205, LEU271, TYR303	GLY97, GLU98, CYS100, PHE150, PHE205, LEU271,
HDAC2	SAHA	GLY32, HIS33, PRO34, GLU103, ASP104, GLY154, PHE155, HIS183, PHE210, LEU276	HIS33, PRO34, ASP104, GLY154, PHE155, HIS183, PHE210, LEU276
	3-Cl SAHA	HIS33, PRO34, GLU103, ASP104, GLY154, PHE155, HIS183, PHE210, LEU276, TYR308	HIS33, PRO34, GLY154, PHE155, HIS183, PHE210, LEU276
	3-Cl, 4-F SAHA	GLU76, LYS79, PHE80, ARG82, SER83, TYR92, GLN95, ARG98, PHE99	GLU76, PHE80, TYR92, GLN95, PHE99
HDAC3	SAHA	HIS22, PRO23, ASP92, ASP93, GLY143, PHE144, HIS172, PHE200, LEU266	HIS22, PRO23, GLY143, PHE144, HIS172, PHE200, LEU266
	3-Cl SAHA	TYR9, PRO11, ASN15, HIS27, ALA30, HIS33, SER34, LEU37, HIS38, GLU327, TYR328	TYR9, HIS27, ALA30, SER34, LEU37, GLU327
	3-Cl, 4-F SAHA	GLY21, HIS22, PRO23, GLY91, ASP92, ASP93, GLY143, PHE144, HIS172, PHE200, LEU266	GLY21, PRO23, ASP93, PHE144, HIS172, LEU266
HDAC8	SAHA	LEU14, PRO16, LYS132, VAL133, LEU892, GLN295, VAL321, ILE322, LEU323, GLY324	LEU14, PRO16, LYS132, VAL133, LEU292, GLN295, LEU323, GLY324
	3-Cl SAHA	LYS33, ILE34, HIS143, GLY151, PHE152, HIS180, MET274, PHE208, TYR306	ILE34, GLY151, PHE152, HIS180, MET274, PHE208, TYR306
	3-Cl, 4F SAHA	ALA270, GLY271, ASN307, ALA309, ASN310, ARG313, ALA339, GLY341, PRO342, ASP343, GLU347, ILE348, THR349, SER351	ALA270, GLY271, ASN310, PRO342, GLU347, ILE348,

Note: SAHA-Suberoyl anilide hydroxamic acid, 3-Cl SAHA = 3-Chloro SAHA; 3-Cl, 4F SAHA = 3-Chloro-4-Fluoro SAHA.

Table 5
H-Bond interactions of SAHA and novel analogs against class I HDACs.

Protein name	Drug/ analog	Interaction	Distance (Å)
HDAC1	SAHA	NE2 atom of HIS178 with O2 atom of SAHA	3.11
		N atom of PHE205 with O2 atom of SAHA	3.21
	3-Cl SAHA	C atom of HIS57 with O3 atom of Cl SAHA	3.08
	3-Cl, 4-F SAHA	OD1 atom of ASN95 with N2 atom of F,Cl SAHA	3.16
		N atom of ASP99 with O3 atom ofF,Cl SAHA	3.02
		N atom of GLY149 with O2 atom ofF, Cl SAHA	3.29
HDAC2	SAHA	O atom of GLU103 with N2 atom of SAHA	3.05
	3-Cl SAHA	OE1 atom of GLU103 with O3 atom of Cl SAHA	3.06
		OD1 atom of ASP104 with O3 atom of Cl SAHA	2.81
	3-Cl, 4-F SAHA	O atom of LYS79 with O3 atom ofF,Cl SAHA	3.04
		NE atom of ARG82 with O3 atom ofF, Cl SAHA	2.92
		OG atom of SER83 with O1 atom of F, ClSAHA	2.96
		OG atom of SER83 with N1 atom ofF, Cl SAHA	3.33
		OG atom of SER83 with N2 atom of F, ClSAHA	3.02
HDAC3	SAHA	OD1 atom of ASP92 with N2 atom of SAHA	3.07
		OD1 atom of ASP93 with O3 atom of SAHA	2.93
	3-Cl SAHA	O atom of PRO11 with O3 atom of Cl SAHA	3.19
		OD1 atom of ASN15 with N2 atom of Cl SAHA	3.07
		ND2 atom of HIS33 with O3 atom of Cl SAHA	2.91
		ND1 atom of HIS33 with O1 atom of Cl SAHA	3.18
		OH atom of TYR328 with O2 atom of Cl SAHA	2.86
	3-Cl, 4-F SAHA	ND1 atom of HIS22 with O2 atom of F,ClSAHA	3.12
		O atom of ASP92 with N2 atom of F, ClSAHA	2.80
		OD1 atom of ASP92 with O3 atom of F,ClSAHA	3.01
HDAC8	SAHA	O atom of VAL321 with N2 atom of SAHA	3.16
		O atom of ILE322 with O3 atom of SAHA	2.76
	3-Cl SAHA	O atom of LYS33 with O3 atom of Cl SAHA	3.07
	3-Cl, 4-F SAHA	ND2 atom of ASN307 with O2 atom ofF,Cl SAHA	2.84
		NH2 atom of ARG313 with O3 atom of F, Cl SAHA	3.08
		O atom of GLY341 with O3 atom of F, Cl SAHA	2.90
		O atom of THR349 with N1 atom of F, Cl SAHA	2.85
		OG atom of SER351 with O1 atom of F, Cl SAHA	3.04

Note: SAHA=Suberoyl anilide hydroxamic acid, 3-Cl SAHA = 3-Chloro SAHA; 3-Cl, 4-F SAHA = 3-Chloro-4-Fluoro SAHA.

breast cancer metastasis [32–34]. In the study, the effect of various SAHA analogs at the CAP region such as 3-chloro SAHA, 3-chloro-4--fluoro SAHA, 2-bromo SAHA, 4- bromo SAHA, 3,5-dimethyl SAHA, 3-methyl-4-bromoSAHA, 2-aminothiazole SAHA, 2-amino pyrimidine SAHA were examined (Fig. 1). SAHA analogs have induced cytotoxicity in U87MG cancer cells at 2 μM, and 4 μM. These analogs also induced cytotoxic effects in MCF-7 breast cancer cells at 0.5 μM concentration. Interestingly, these SAHA analogs caused an inhibitory effect on cell viability in chronic lymphoid leukemia cells (CLL) such as Raji, and Daudi at 64 μM, and 128 μM concentrations (Fig. 2). It was evident CLL cancer cells exhibit loss of p53 allele due to del 17p chromosome or mutation in p53 [35,36]. Also, the mutation causes loss of tumor-suppressive function of p53 leading to cancer cell growth, and proliferation.

The HDAC-8 induce epithelial to mesenchymal transition *via* AKT/GSKβ/Snail signals [37]. Similarly, studies have indicated like hematological malignancies such as acute myeloid leukemia (AML) (i. e. HL-60, and THP-1) that lacks p53 tumor suppressor was sensitive to chemotherapeutic drugs and enhanced cytotoxicity due to the inhibition of HDAC-8. Studies by [38] have indicated over expression of HDAC-8 modifies non-histone protein such as p53 in AML. Also, they found that HDAC-8 inhibition leads to inhibition of cancer cell proliferation *via* inhibition of Wnt pathway. HDAC-8 inhibitor (PCI-34051) was found to inhibit the T-cell lymhoma [39]. Similarly, in B-CLL patients it was

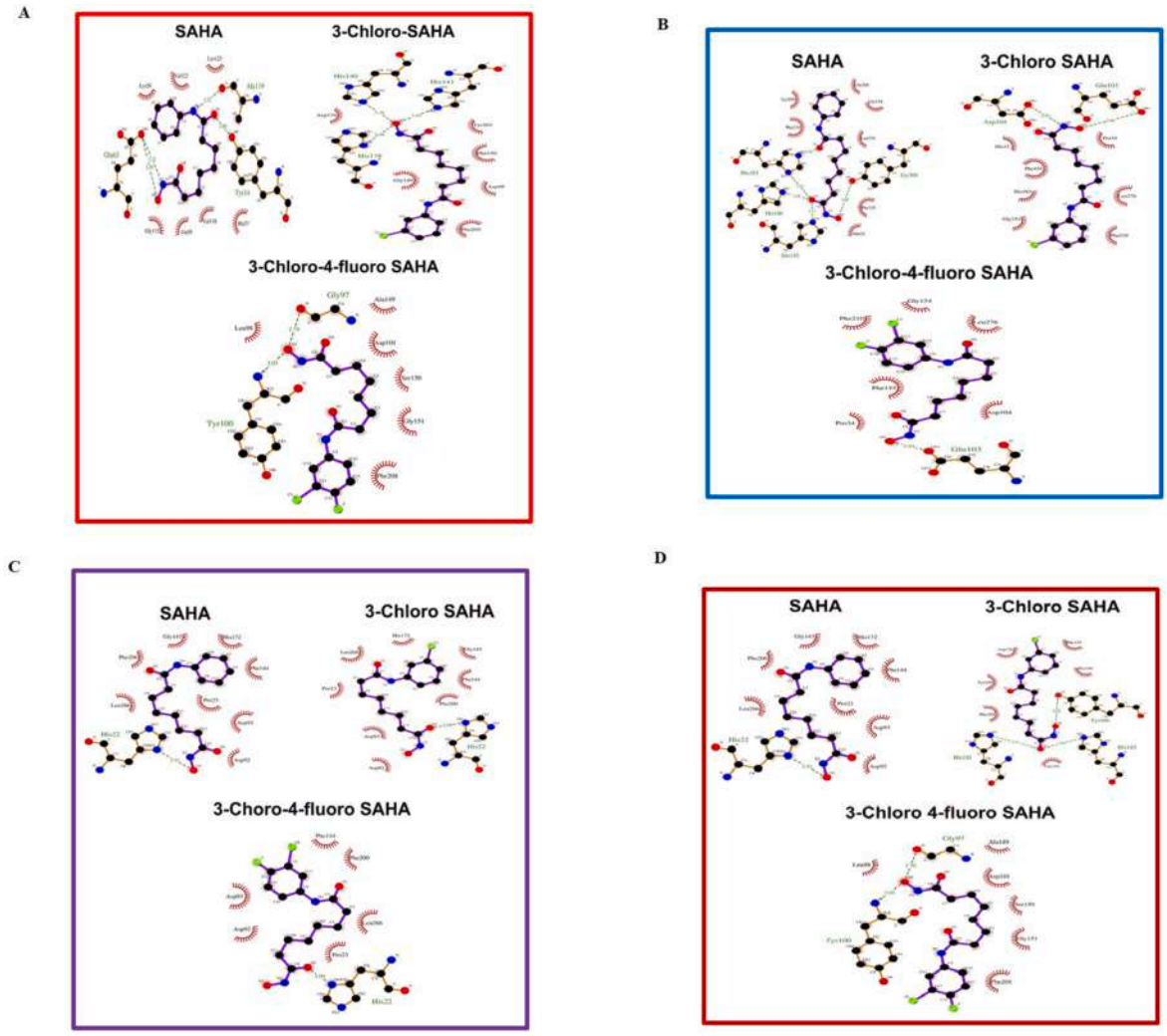

Fig. 6. SAHA and HDAC interaction study using Lig plot + program (6a). The 2D ligplot interaction models of SAHA, 3-Chloro SAHA, and 3-Chloro, 4-Fluoro SAHA with HDAC-1 show their hydrogen bond interactions and other electrostatic interactions between residues and atoms of HDAC1 and ligands respectively. The H-bond interactions between the HDAC1 residues and ligands atoms were clearly shown along with the bond distance. **(6b).** The 2D lig plot interaction models of SAHA, 3-chloro SAHA, and 3-Chloro, 4-Fluoro SAHA with HDAC-2 shows their hydrogen bond interactions and other electrostatic interactions between residues and atoms of HDAC2 and ligands respectively. The H-bond interactions between the HDAC2 residues and ligands atoms were clearly shown along with the bond distance. **(6c).** The 2D lig plot interaction models of SAHA, 3-Chloro SAHA, and 3-Chloro, 4-Fluoro SAHA with HDAC-3 shows their hydrogen bond interactions and other electrostatic interactions between residues and atoms of HDAC3 and ligands respectively. The H-bond interactions between the HDAC3 residues and ligands atoms were clearly shown along with the bond distance. **(6d).** The 2D ligplot interaction models of SAHA, 3-Chloro SAHA, and 3-Chloro, 4-Fluoro SAHA with HDAC-8 show their hydrogen bond interactions and other electrostatic interactions between residues and atoms of HDAC8 and ligands respectively. The H-bond interactions between the HDAC8 residues and ligands atoms were clearly shown along with the bond distance.

observed that p53 is mutated and Bcl-2 is over expressed and result in chemo-resistance. Thus, inhibition of HDAC-8 is useful strategy to inhibit the leukemia, and neuroblastoma (NB). In addition, inhibition of HDAC class I genes lead to inhibition of leukemia and NB [40]. Finally, in B-cll Bruton's tyrosine kinase (BTK) and HDAC cooperate in causing cancer aggressiveness. Thus, we were interested to study both Raji (B-CLL), and MCF-7 (breast cancer) cell lines also in the study. Cancer cells with mutant p53 have exhibited loss of tumor suppressor function, and participate in tumor aggressiveness [41]. Emerging studies have indicated that HDAC inhibitors that inhibit HDAC-8 activity restores mutant p53 to wild-type function. Frequent p53 and Pten mutations in mouse CNS have indicated the penetrant acute-onset high grade glioma similar to human primary glioma [42]. Till date studies have synthesized SAHA analogs and these are not similar except 4-Br SAHA that inhibit liver cancer (Chatla et al., 2016), Here we have synthesized and focussed substitutions fully on cap region of SAHA parent molecules with various new modifications such as 3,5-dimethyl, single chloro (i. e.3-Choro substitution), aminothiazole, 3-methyl 4-bromo, 2-aminiothiazole, 2-aminopyridine etc which were not studied yet. Till date these substitutions were not explored on GBM. We found these analogs were found to be highly cytotoxic, induce apoptosis at lower concentration, inhibit HDAC-8 activity very effectively in GBM cancer cells and thus very much useful for GBM cancer therapy. Also, HDAC-8 inhibition leads to a decrease in O6-methyl-guanine DNA methyltransferase (MGMT) protein level leading to the effective killing of tumor cells and thus these molecules can be employed in temozolomide resistant GBM patients [43–45]. Our study have indicated profound inhibition of HDAC-8 activity in SAHA analog treated GBM B-CLL (Raji), and MCF-7 cancer cells (Fig. 3). In general, HDAC inhibitors modulate cell-cycle arrest, and apoptosis [26]. Furthermore, these potent analogs were tested for their apoptotic inducing ability in GBM cancer cells. We observed 3-chloro-4--fluoro SAHA was found to be highly effective in inducing apoptosis, as well as colony-forming ability (Fig. 4a and b). Emerging studies have shown also indicated that histone deacetylase inhibitors that can

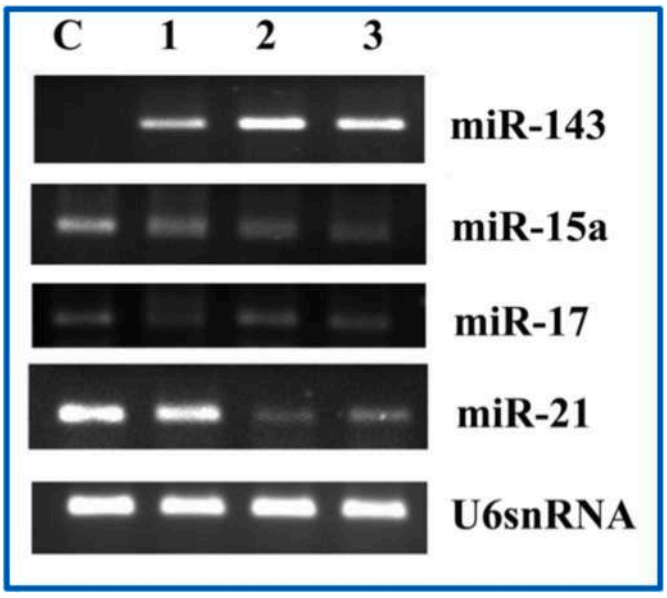

Fig. 7. Effect of SAHA analogs on microRNA expression in U87MG cells. The U87MG cells were treated with potent SAHA analogs at 4 μM for 24h. This was followed by small RNA isolation by using Qiagen columns and then subjected to RT-PCR using miRNA-specific primers. Here U6SnRNA was used as a control. C: Control cells without any treatment. **1:** SAHA; **2**: 3-Chloro SAHA; **3:** 3 = Chloro-4-fluoro SAHA.

modulate class I HDAC gene expression was considered as potent anti-cancer molecules. We have examined the effect of potent SAHA analogs on the expression of class I HDAC genes such as HDAC-1, HDAC-2, HDAC-3, and HDAC-8 as well as p53, and PTEN tumor suppressor genes in U87MG Glioblastoma cancer cells. We observed 3-Chloro SAHA, 3-Chloro-4-fluoro SAHA have exhibited a significant inhibitory effect on the gene expression of HDAC-2, and HDAC-3. Compound especially 3-Chloro-4-fluoro SAHA treatment induced p53 gene expression by 2-folds (Fig. 5). Studies have also indicated that small molecules that target the Blood-brain barrier, as well as that can inhibit GBM, and CLL cancers are of the urgent need for therapy against GBM, and CLL cancers due to their heterogeneous, highly proliferative, as well as chemo-resistant [46]. Furthermore, these potent molecules bind to HDAC-1, HDAC-2, HDAC-3, and HDAC-8 and have exhibited high binding energies as observed by LigPlot + program (Fig. 6).

Epigenetic mechanisms were considered as the key factors involved in the pathogenesis of cancers such as glioblastoma which is chemo-resistant, aggressive in nature [47]. Studies have indicated that HDAC inhibitors, and microRNAs regulate each other in dictating cancer phenotype [48]. Also, emerging studies have clearly indicated the role of Rictor, the component of mammalian target of Rapamycin 2 (mTORC2) in enhancing cancer metabolism, and cancer proliferation by regulation of chromatin epigenetics in cancer cells [27]. Studies by Ref. [49] have indicated the potential role of HDAC inhibitors in the regulation of tumor cell metabolism *via* a decrease in Myc gene, and glycolytic genes. Thus, we have tested Rictor gene expression in SAHA treated U87MG cancer cells. Results have shown the decreased expression of Rictor (Figure -5). MicroRNA expression studies have indicated that these analogs upregulated tumor suppressor microRNAs such as miR-15–3p, miR-143, and decreased the expression of a miR-21 oncogene (Fig. 7). Interestingly, the potent molecules such as 3-Chloro SAHA, 3-chloro 4-fluoro SAHA have exhibited good ADME properties and have followed Lipinski rule of Five. Thus, these SAHA analogs can be further needed to be studied by *In vivo* studies.

5. Conclusion

In the present study, we have investigated the novel SAHA analogs on the cell viability was analyzed using U87MG (GBM), Raji (CLL), and MCF-7 (breast cancer) cells. These compounds were found to be highly cytotoxic against cancer cells. Furthermore, these compounds were tested for their ability to modulate the histone deacetylase-8 enzyme as well as class I HDAC gene expression. We found that these molecules enhanced the expression of HDAC-2, HDAC-3, and inhibited HDAC-8 activity. These SAHA analogs were found to induce apoptosis *via* decreasing the Rictor, a crucial component of the mTORC2 complex involved in regulating cancer cell metabolism, as well as modulating the microRNA gene expression in U87MG cells. Interestingly, these molecules interact with class I HDACs and exhibited high binding energies (Δ G values), as well as possessed good solubility, and can pass blood-brain barrier (BBB). Compounds that inhibit HDAC-8 is urgent demand for treating GBM and CLL cancers and thus these molecules can be further needed to be investigated in clinics.

Credit author statement

Janaki Ramaiah Mekala, the corresponding author has conceived the idea, written the paper, conducted the biological experiments, and guided the research. Prasanna Srinivasan Ramalingam has conducted modelling studies as well as few biological studies such as Westernblot analysis. Kurappalli Rohil Kumar has worked on MTT Assay in Raji cells MicroRNA expression studies, and HDAC gene expression. Sivagami Mathavan has synthesized the organic compounds. Dr. YBRD Rajesh has guided in synthesis of organic molecules. Nageswara Rao Moparthi and Rajasekhar Reddy Manyam has worked modelling aspects and helped in the writing the manuscript.

Declaration of competing interest

The authors declare the following financial interests/personal relationships which may be considered as potential competing interests:

Acknowledgments

Corresponding author is thankful to Department of Biotechnology (DBT) for financial support for the project file No: BT/PR20836/MED/30/1727/2016, Ministry of Science & technology; Science & engineering Research Board (SERB) for financial support for the project file No: EMR/2017/001201, and thanks to SASTRA management for the infrastructure and facilities. Authors would also like to thankful to the management of Koneru Lakshmaiah Education Foundation (KLEF), Green Fields, Vaddeswaram, Guntur for the excellent infrastructure, and constant encouragement.

Appendix A. Supplementary data

Supplementary data to this article can be found online at https://doi.org/10.1016/j.cbi.2022.109876.

References

[1] R. Benedetti, M. Conte, L. Altucci, Targeting histone deacetylases in diseases: where are We? Antioxids & red, Sign 23 (1) (2020) 99–126, https://doi.org/10.1089/ars.2013.5776.
[2] S.Y. Park, J.S. Kim, A short guide to histone deacetylases including recent progress on class II enzymes, Exp. Mol. Med. 52 (2020) 204–212, https://doi.org/10.1038/s12276-020-0382-4.
[3] E. Ceccacci, S. Minucci, Inhibition of histone deacetylases in cancer therapy: lessons from leukaemia, Br. J. Cancer 114 (6) (2016) 605–611, https://doi.org/10.1038/bjc.2016.36.
[4] G. Li, Y. Tian, W.G. Zhu, The roles of histone deacetylases and their inhibitors in cancer therapy, Front. Cell Dev. Biol. 8 (2020) 1004, https://doi.org/10.3389/fcell.2020.576946.

[5] T. Eckschlager, J. Plch, M. Stiborova, J. Hrabeta, Histone deacetylase inhibitors as anticancer drugs, Int. J. Mol. Sci. 18 (7) (2017) 1414, https://doi.org/10.3390/ijms18071414.

[6] C. Srinivas, V. Swathi, C. Priyanka, T. Anjana Devi, B.V. Subba Reddy, M. Janaki Ramaiah, U. Bhadra, M.P. Bhadra, Novel SAHA analogues inhibit HDACs, induce apoptosis and modulate the expression of microRNAs in hepatocellular carcinoma, Apoptosis 21 (11) (2016) 1249–1264, https://doi.org/10.1007/s10495-016-1278-6.

[7] J.Y. Lee, C.W. Kuo, S.L. Tsai, S.M. Cheng, S.H. Chen, H.H. Chan, C.H. Lin, K.Y. Lin, C.F. Li, J.R. Kanwar, E.Y. Leung, C.C. Cheung, W.J. Huang, Y.C. Wang, C. H. Cheung, Inhibition of HDAC3- and HDAC6-promoted survivin expression plays an important role in SAHA-induced autophagy and viability reduction in breast cancer cells, Front. Pharmacol. 7 (2016) 81, https://doi.org/10.3389/fphar.2016.00081.

[8] M. Rabe, S. Dumont, A. Alvarez-Arenas, H. Janati, J. Belmonte-Beitia, G.F. Calvo, C. Thibault-Carpentier, Q. Sery, C. Chauvin, N. Joalland, F. Briand, S. Blandin, E. Scotet, C. Pecqueur, J. Clairambault, L. Oliver, V. Perez-Garcia, A. Nadaradjane, P.F. Cartron, C. Gratas, F.M. Vallette, Identification of a transient state during the acquisition of temozolomide resistance in glioblastoma, Cell Death Dis. 11 (1) (2020) 19, https://doi.org/10.1038/s41419-019-2200-2.

[9] K. Lohitesh, H. Saini, A. Srivastava, S. Mukherjee, A. Roy, R. Chowdhury, Autophagy inhibition potentiates SAHA-mediated apoptosis in glioblastoma cells by accumulation of damaged mitochondria, Oncol. Rep. 39 (6) (2018) 2787–2796, https://doi.org/10.3892/or.2018.6373.

[10] V. Richon, Cancer biology: mechanism of antitumour action of vorinostat (suberoylanilide hydroxamic acid), a novel histone deacetylase inhibitor, Br. J. Cancer 95 (2006) S2–S6, https://doi.org/10.1038/sj.bjc.6603463.

[11] J. Auzmendi-Iriarte, A. Saenz-Antonanzas, I. Mikelez-Alonso, E. Carrasco-Garcia, M. Tellaetxe-Abete, C.H. Lawrie, N. Sampron, A.L. Cortajarena, A. Matheu, Characterization of a new small-molecule inhibitor of HDAC6 in glioblastoma, Cell Death Dis. 11 (6) (2020) 417, https://doi.org/10.1038/s41419-020-2586-x.

[12] H. Was, S.K. Krol, D. Rotili, A. Mai, B. Wojtas, B. Kaminska, M. Maleszewska, Histone deacetylase inhibitors exert anti-tumor effects on human adherent and stem-like glioma cells, Clin. Epigenet. 11 (2019) 11, https://doi.org/10.1186/s13148-018-0598-5.

[13] M. Eckert, L. Klumpp, r S.M. Hube, Cellular effects of the antiepileptic drug valproic acid in glioblastoma, Cell. Physiol. Biochem. 44 (4) (2017) 1591–1605, https://doi.org/10.1159/000485753.

[14] M.T. Laws, R.E. Bonomi, S. Kamal, D.J. Gelovani, J. Llaniguez, S. Potukutchi, X. Lu, T. Mangner, J.G. Gelovani, Molecular imaging HDACs class IIa expression-activity and pharmacologic inhibition in intracerebral glioma models in rats using PET/CT/(MRI) with [18F] TFAHA, Sci. Rep. 9 (1) (2019) 3595, https://doi.org/10.1038/s41598-019-40054-2.

[15] M.A. Choi, S.Y. Park, H.Y. Chae, Y. Song, C. Sharma, Y.H. Seo, Design, synthesis and biological evaluation of a series of CNS penetrant HDAC inhibitors structurally derived from amyloid-β probes, Sci. Rep. 9 (1) (2019) 13187, https://doi.org/10.1038/s41598-019-49784-9.

[16] R.G. Reddy, U.A. Bhat, S. Chakravarty, A. Kumar, Advances in histone deacetylase inhibitors in targeting glioblastoma stem cells, Cancer Chemother. Pharmacol. 86 (2) (2020) 165–179, https://doi.org/10.1007/s00280-020-04109-w.

[17] J.R. Mekala, S.M. Naushad, L. Ponnusamy, G. Arivazhagan, V. Sakthiprasad, M. Pal-Bhadra, Epigenetic regulation of miR-200 as the potential strategy for the therapy against triple-negative breast cancer, Gene 641 (2018) 248–258, https://doi.org/10.1016/j.gene.2017.10.018.

[18] M.J. Ramaiah, Functions and epigenetic aspects of miR15/16: possible future cancer therapeutics, Gene Rep. 12 (2018) 149–164, https://doi.org/10.1016/j.genrep.2018.06.012.

[19] M.J. Ramaiah, mTOR inhibition and p53 activation, microRNAs: the possible therapy against pandemic COVID-19, Gene Rep 20 (2020) 100765, https://doi.org/10.1016/j.genrep.2020.100765.

[20] M. Janaki Ramaiah, P. Jaya Vasavi, N. Venkata Chandana, Potentials of miR-15/16 targeting cancer stem cell pathways: novel implication in cancer chemotherapy, Gene Rep 20 (2020) 100755, https://doi.org/10.1016/j.genrep.2020.100755.

[21] J.R. Mekala, R.K. Kurappalli, P.S. Ramalingam, N.R. Moparthi, N-acetyl l-aspartate and Triacetin modulate tumor suppressor MicroRNA and class I and II HDAC gene expression induce apoptosis in Glioblastoma cancer cells in vitro, Life Sci. 286 (2021) 120024, https://doi.org/10.1016/j.lfs.2021.120024.

[22] X. Liu, X. Chen, X. Yu, Y. Tao, A.M. Bode, Z. Dong, Y. Cao, Regulation of microRNAs by epigenetics and their interplay involved in cancer, J. Exp. Clin. Cancer Res. 32 (1) (2013) 96, https://doi.org/10.1186/1756-9966-32-96.

[23] A. Conti, M. Aguennouz, D. La Torre, C. Tomasello, S. Cardali, F.F. Angileri, F. Maio, A. Cama, A. Germano, G. Vita, F. Tomasello, miR-21 and 221 upregulation and miR-181b downregulation in human grade II-IV astrocytic tumors, J. Neuro Oncol. 93 (3) (2009) 325–332, https://doi.org/10.1007/s11060-009-9797-4.

[24] J. Wang, H. Liu, L. Tian, F. Wang, L. Han, W. Zhang, Y.A. Bai, miR-15b inhibits the progression of glioblastoma cells through targeting insulin-like growth factor receptor 1, Horm Cancer 8 (1) (2017) 49–57, https://doi.org/10.1007/s12672-016-0276-z.

[25] C. Olivier, L. Oliver, L. Lalier, F.M. Vallette, Drug resistance in glioblastoma: the two faces of oxidative stress, Front Mol. Biosci. 7 (2021) 620677, https://doi.org/10.3389/fmolb.2020.620677.

[26] M.J. Ramaiah, A.D. Tangutur, R.R. Manyam, Epigenetic modulation and understanding of HDAC inhibitors in cancer therapy, Life Sci. 277 (2021) 119504, https://doi.org/10.1016/j.lfs.2021.119504.

[27] M. Harachi, K. Masui, H. Honda, Y. Muragaki, T. Kawamata, W.K. Cavenee, P. S. Mischel, N. Shibata, Dual regulation of histone methylation by mTOR complexes controls glioblastoma tumor cell growth via EZH2 and SAM, Mol. Cancer Res. 18 (8) (2020) 1142–1152, https://doi.org/10.1158/1541-7786.MCR-20-0024.

[28] D. Li, N.D. Marchenko, U.M. Mol, SAHA shows preferential cytotoxicity in mutant p53 cancer cells by destabilizing p53 through inhibition of the HDAC-6-HSP90 chaeprone axis, Cell Death Differ. 18 (2011) 1904–1913.

[29] Y.Z. Kim, Altered histone modifications in gliomas, Brain tumor Res. Treat. 2 (2014) 7–21, https://doi.org/10.14796/brtt.2014.2.1.7.

[30] X.F. Yang, Z.J. Zhao, J.J. Liu, X.H. Yang, Y. Gao, S. Zhao, S. Shi, K.Q. Huang, H. C. Zheng, SAHA and/or MG132 reverse the aggressive phenotypes of glioma cells. An Invitro and Vivo study, Oncotarget 8 (2017) 3156–3169, https://doi.org/10.18632/oncotarget.13680.

[31] A.T. Negmeldin, J.R. Knoff, M.K.H. Pfum, The structural requirements of histone deacetylase inhibitors. C4-modified SAHA analogs display dual HDAC-6/HDAC-8 slectvity, Eur. J. Med. Chem. 143 (2018) 1790–1806, 10.1016/j.ejmech.2017.10.076.

[32] A.T. Negmeldin, G. Padige, A.V. Bieliauskas, M.K. Pfum, Structural requirements of HDAC inhibitors: SAHA analogues modified at C2 position displayed HDAC-6/8 selectivity, ACS Med. Chem. Lett. 8 (3) (2017) 281–286, https://doi.org/10.1021/acsmedchemlett.6b00124.

[33] S.Y. Park, J.A. Jun, K.J. Jeong, H.J. Heo, J.S. Sohn, H.Y. Lee, C.G. Park, J. Kang, Histone deacetylases 1,6, and 8 are critical for invasion in breast cancer, Oncol. Rep. 25 (6) (2011) 1677–1681, https://doi.org/10.3892/or.2011.1236.

[34] D.E. Oslon, F.F. Wagner, T. Kaya, J.P. Gale, N. Aidoud, E.L. Davoine, F. Lazzaro, M. Weiwer, Y.L. Zhang, E.B. Holson, Discovery of the first histone deacetylase 6/8 dual inhibitors, J. Med. Chem. 56 (11) (2013) 4816–4820, https://doi.org/10.1021/jm400390r.

[35] E. Campo, F. Cymbalista, P. Ghia, U. Jäger, S. Pospisilova, R. Rosenquist, A. Schuh, S. Stilgenbauer, TP53 aberrations in chronic lymphocytic leukemia: an overview of the clinical implications of improved diagnostics, Haematologica 103 (12) (2018) 1956–1968, https://doi.org/10.3324/haematol.2018.187583.

[36] T. Zenz, D. Mertens, S. Stilgenbauer, Biological diversity and risk-adapted treatment of chronic lymphocytic leukemia, Haematologica 95 (9) (2010) 1441–1443, https://doi.org/10.3324/haematol.2010.027151.

[37] P. An, F. Chen, Z. Li, Y. Ling, Y. Peng, H. Zhang, J. Li, Z. Chen, H. Wang, HDAC8 promotes the dissemination of breast cancer cells via AKT/GSK-3β/Snail signals, Oncogene 39 (26) (2020) 4956–4969, https://doi.org/10.1038/s41388-020-1337-x.

[38] M. Spreafico, A.M. Gruszka, D. Valli, M. Mazzola, G. Deflorian, A. Quinte, M. G. Totaro, C. Battaglia, M. Alcalay, A. Marozzi, A. Pistocchi, HDAC8: a promising therapeutic target for acute myeloid leukemia, Front. Cell Dev. Biol. 8 (2020) 844, https://doi.org/10.3389/fcell.2020.00844.

[39] S. Balasubramanian, J. Ramos, W. Luo, M. Sirisawad, E. Verner, J.J. Buggy, A novel histone deacetylase 8 (HDAC8)-specific inhibitor PCI-34051 induces apoptosis in T-cell lymphomas, Leukemia 22 (2008) 1026–1034, https://doi.org/10.1038/leu.2008.9.

[40] E. Vagapova, M. Kozlov, T. Lebedev, K. Ivanenko, O. Leonova, V. Popenko, P. Spirin, S. Kochetkov, V. Prassolov, Selective inhibition of HDAC class I sensitizes leukemia and Neuroblastoma cells to anti-cancer drugs, Biomedicines 9 (12) (2021) 1846, https://doi.org/10.3390/biomedicines9121846.

[41] P.A. Muller, K.H. Vousden, Mutant p53 in cancer: new functions and therapeutic opportunities, Cancer Cell 25 (3) (2014) 304–317, https://doi.org/10.1016/j.ccr.2014.01.021.

[42] H.W. Zheng, H. Ying, H. Yan, A.C. Kimmelman, D.J. Hiller, A.-J. Chen, et al., P53 and Pten control neural and glioma stem/progenitor cell renewal and differentiation, Nature 455 (7216) (2008) 1129–1133, https://doi.org/10.1038/nature07443.

[43] M.A. Dawson, T. Kouzarides, Cancer epigenetics: from mechanism to therapy, Cell 150 (1) (2012) 12–27, https://doi.org/10.1016/j.cell.2012.06.013.

[44] A.C. West, R.W. Johnstone, New and emerging HDAC inhibitors for cancer treatment, J. Clin. Invest. 124 (1) (2014) 30–39, https://doi.org/10.1172/JCI69738.

[45] I. Santos-Barriopedro, Y. Li, S. Bahl, E. Seto, HDAC8 affects MGMT levels in glioblastoma cell lines via interaction with the proteasome receptor ADRM1, Genes Cancer 10 (5–6) (2019) 119–133, https://doi.org/10.18632/genesandcancer.197.

[46] B. Xiong, Y. Wang, Y. Chen, S. Xing, Q. Liao, Y. Chen, Q. Li, W. Li, H. Sun, Strategies for structural modification of small molecules to improve blood-brain barrier penetration: a recent perspective, J. Med. Chem. 64 (18) (2021) 13152–13173, https://doi.org/10.1021/acs.jmedchem.1c00910.

[47] P. Bezecny, Histone deacetylase inhibitors in glioblastoma: pre-clinical and clinical experience, Med. Oncol. 31 (6) (2014) 985, https://doi.org/10.1007/s12032-014-0985-5.

[48] S.R. Ali, K.J. Humphreys, R.A. McKinnon, M.Z. Michael, Impact of histone deacetylase inhibitors on microRNA expression and cancer therapy: a review, Drug Dev. Res. 76 (6) (2015) 296–317, https://doi.org/10.1002/ddr.21268.

[49] T.T.T. Nguyen, Y. Zhang, E. Shang, C. Shu, C. Torrini, J. Zhao, E. Bianchetti, A. Mela, N. Humala, A. Mahajan, A.O. Harmanci, Z. Lei, M. Maienschein-Cline, C. M. Quinzii, M.A. Westhoff, G. Karpel-Massler, J.N. Bruce, P. Canoll, M.D. Siegelin, HDAC inhibitors elicit metabolic reprogramming by targeting super-enhancers in glioblastoma models, J. Clin. Invest. 130 (7) (2020) 3699–3716, https://doi.org/10.1172/JCI129049.